Title
Fully Automated Heart Disease Diagnosis and Evaluation using a Phonocardiogram-Based System

Author
Saraf, Kanav

Publication Date
2020

Peer reviewed|Thesis/dissertation

UNIVERSITY OF CALIFORNIA

Los Angeles

Fully Automated Heart Disease Diagnosis and Evaluation using a Phonocardiogram-Based System

A dissertation submitted in partial satisfaction of the requirements for the degree Doctor of Philosophy in Bioengineering

by

Kanav Saraf

2020

ABSTRACT OF THE DISSERTATION

Fully Automated
Heart Disease Diagnosis and Evaluation
using a Phonocardiogram-Based System

by

Kanav Saraf
Doctor of Philosophy in Bioengineering
University of California, Los Angeles, 2020
Professor William J. Kaiser, Co-Chair
Professor Jacob J. Schmidt, Co-Chair

Individuals with undiagnosed heart disease and those unable to seek advanced care for existing heart-disease related disabilities face a risk of premature death. Guidelines released by the American Heart Association aim to increase healthy life expectancy in such individuals over the next decade. Timely diagnosis and evaluation of heart disease in these individuals with existing tools is a challenge, especially in low-resource primary care settings. Presented here is a computer-aided heart-sound-based system that carries the potential to overcome this challenge and provide these individuals with the opportunity to pursue an accelerated path of care to recovery. This system analyzes phonocardiogram signals collected using acoustic sensors to identify variations in cardiac physiology that are otherwise measured by resource-intensive imaging tools.

Signal acquisition is noninvasive, and the entire system operates in a fully automated manner without requirements of training or expert supervision. The acquired signal waveforms are processed using filtering, noise subtraction, heartbeat segmentation, and heartbeat quality assurance algorithms to extract physiologically motivated features for heart disease diagnosis and evaluation. The system and its algorithms were developed and validated using real-world heart sound data from hospital inpatients. When tested on 96 inpatients at the Ronald Reagan University of California Los Angeles Medical Center, the system was able to identify aortic stenosis with a sensitivity and specificity of 92% and 95%. When tested on 34 inpatients being evaluated for heart failure at the Oregon Health & Science University Hospital, the system was able to generate echocardiography-like parameters for left ventricular diastolic function and left atrial pressure evaluation with accuracies of 87.5% and 75%. These results demonstrate the potential of this phonocardiogram-based system in providing clinically relevant heart disease diagnosis and evaluation at the point of primary care and in fulfilling the immediate critical need for improving outcomes in at-risk individuals.

The dissertation of Kanav Saraf is approved.

Aman Mahajan

Gregory J. Pottie

Chih-Kong Ken Yang

Jacob J. Schmidt, Committee Co-Chair

William J. Kaiser, Committee Co-Chair

University of California, Los Angeles

2020

CONTENTS

FIGURES

TABLES

ACRONYMS

A	Standardized systolic amplitude feature
A_{norm}	Vector of systolic amplitude estimates normalized by noise floor
ASE	American Society of Echocardiography
A_{sys}	Vector of systolic amplitude estimates
AUC	Area Under the Curve
d_{sys}	Systolic signal segment
EACVI	European Association of Cardiovascular Imaging
f_{com}	Vector of systolic high-frequency estimates
F_{com}	Standardized systolic frequency feature
ROC	Receiver Operating Characteristic
S1	First heart sound
S2	Second heart sound

ACKNOWLEDGEMENTS

I am grateful to Professor William Kaiser and Dr. Aman Mahajan for the opportunity to work on this research project under their guidance. Their vision for the future continues to inspire me. I am deeply indebted to them for their support and encouragement throughout my education.

Thank you to Professor Jacob Schmidt, Professor Gregory Pottie, and Professor Chih-Kong Ken Yang for their oversight, guidance, and time as part of my doctoral committee.

Thank you to Henrik Borgstrom for sharing his insight, feedback, and advice at each stage of the project. His mentorship has been pivotal in my academic and professional development.

Thank you to Peter Borgstrom, Chris Baek, Michael Wasko, Xu Zhang, and Yi Zheng for their valuable contributions without which this research would not have been possible.

VITA

2016 Master of Science in Bioengineering

University of California, Los Angeles

2015 Bachelor of Science in Bioengineering

University of California, Los Angeles

K. Saraf et al., "Assessment of Left Ventricular Diastolic Function using Phonocardiogram Signals: A Comparison with Echocardiography," *2020 42nd Annual International Conference of the IEEE Engineering in Medicine and Biology Society (EMBC)*, submitted for publication, 2020.

K. Saraf et al., "Fully-Automated Mitral E/A Ratio Computation Using a Phonocardiogram-Based Feature," *Journal of the American College of Cardiology*, vol. 75, no. 11, pp. 3503, 2020.

C. I. Baek et al., "Poster Abstract: Automated Detection of the Onset of Ventricular Depolarization in Challenging Clinical ECG Data," *2019 IEEE/ACM International Conference on Connected Health: Applications, Systems and Engineering Technologies (CHASE)*, pp. 9-10, 2019.

K. Saraf et al., "Fully-Automated Diagnosis of Aortic Stenosis Using Phonocardiogram-Based Features," *2019 41st Annual International Conference of the IEEE Engineering in Medicine and Biology Society (EMBC)*, pp. 6673-6676, 2019.

CHAPTER 1

INTRODUCTION

1.1 Structure and Function of the Heart

The human heart is a fist-sized muscular organ located in the thoracic cavity in between the lungs [1]. Its muscle walls are composed of connective tissue and specialized cardiac muscle tissue. The walls enclose an internal cavity that can be divided into four chambers: right atrium, right ventricle, left atrium, and left ventricle (Figure 1-1). Each atrium is thin walled and acts as a primer pump for the ventricles, and each ventricle is thick walled and provides the main pumping action to propel blood. On the right side of the heart, deoxygenated blood from the organs arrives into the right atrium via the vena cava. This blood then enters the right ventricle from where it is circulated to the lungs for oxygenation via the pulmonary artery. On the left side of the heart, oxygenated blood from the lungs enters the left atrium via the pulmonary vein. This blood then moves into the left ventricle from where it is pumped out to the rest of the body via the aorta. The unidirectional nature of this blood flow is maintained by four heart valves: two

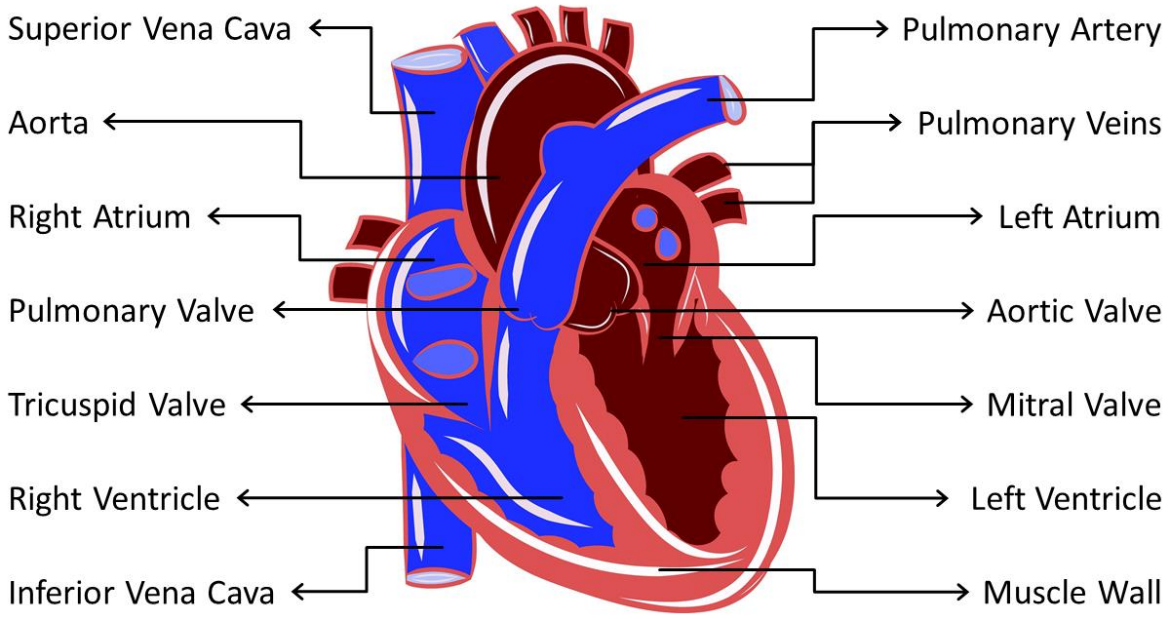

Figure 1-1 Anatomy of the human heart, showing four chambers (right atrium, right ventricle, left atrium, and left ventricle), four major blood vessels (vena cava, pulmonary artery, pulmonary vein, and aorta), and four heart valves (tricuspid, pulmonary, mitral, and aortic). The right side of the heart pumps deoxygenated blood (blue) to the lungs and the left side pumps oxygenated blood (red) to the rest of the body.

atrioventricular valves (i.e., the tricuspid and mitral valves) between each atrium and ventricle, and two semilunar valves (i.e., the pulmonary and aortic valves) at the base of vessels leaving the ventricles. A small portion of the oxygenated blood flowing out of the aorta is also redirected to be supplied to the muscles of the heart via the coronary arteries.

The series of events that take place from the start of one heartbeat to the next constitute the cardiac cycle [1] (Figure 1-2). The rhythmic nature of this cycle is controlled by a specialized neural conduction system that stimulates cardiac muscle tissue to contract. The action potential for contraction is initiated at the sinoatrial node

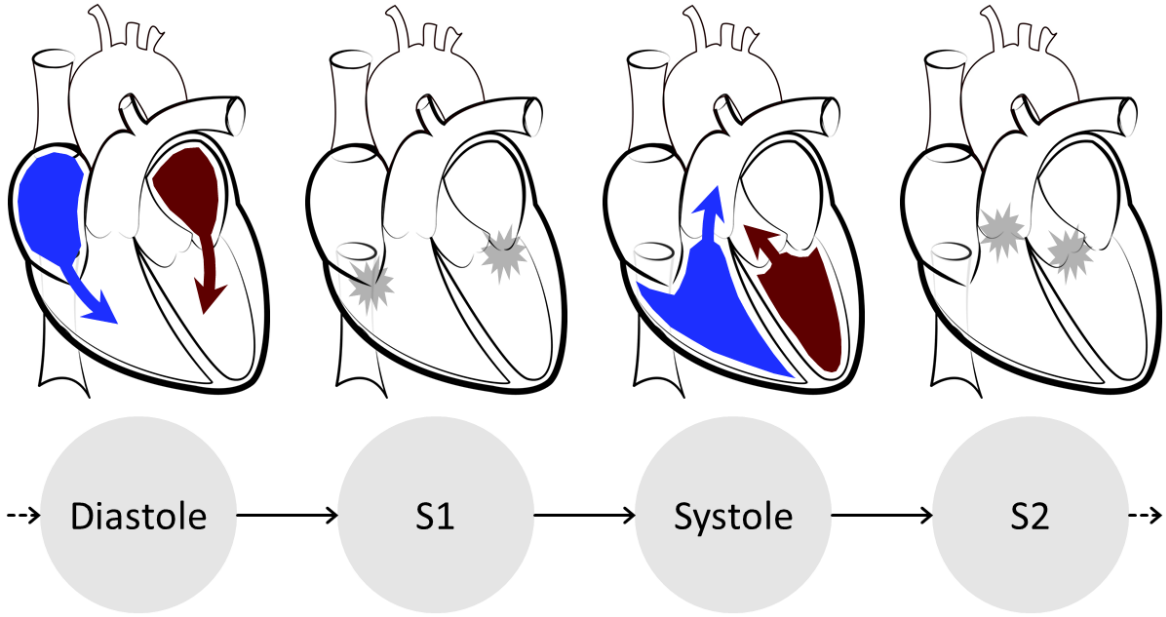

Figure 1-2 Phases of the cardiac cycle, showing a period of ventricular filling (diastole), followed by the closure of the tricuspid and mitral valves producing the first heart sound (S1), a period of ventricular contraction (systole), and the closure of the pulmonary and aortic valves producing the second heart sound (S2).

located in the superior wall of the right atrium. This potential is generated roughly 72 times per minute, and travels down to depolarize the atria and ventricles and causes these chambers to contract one after the other. The contraction of the atria leads to ventricular filling, and this period of the cardiac cycle is referred to as diastole. Towards the end of diastole, high pressures in the now-filled ventricles cause the tricuspid and mitral valves to close shut, which produces the first heart sound (S1). At the same time, the pulmonary and aortic valves open and the ventricles now contract to push blood out. This period of contraction is referred to as systole. At the end of systole, ventricular relaxation begins, and ventricular pressure drops, which causes the semilunar valves to close shut and

produce the second heart sound (S2). This is closely followed by the re-opening of the tricuspid and mitral valves, and the whole cycle then repeats.

1.2 Diagnosing and Evaluating Heart Disease

Disruptions in the cardiac cycle can reduce the ability of the heart to pump enough blood to meet the body's needs [1]. Such disruptions can be due to structural or functional abnormalities in the heart by birth or acquired during an individual's lifetime. Although the heart has natural mechanisms in place to temporarily compensate for any abnormalities, these can cause severe damage or disease to the heart over time if left untreated (Table 1-1).

Periodic physical examinations at the point of primary care are a quick, safe, and relatively inexpensive way to diagnose heart disease. The goal of such examinations is to confirm the presence of the disease, determine potential causes, and identify any comorbidities. For this purpose, the provider first conducts a thorough review of the individual's medical history. This includes assessment of risk factors for heart disease mortality such as advanced age, physical inactivity, obesity, high-cholesterol diet, high-blood pressure, heavy use of tobacco, and other family history [2]. The provider also looks for signs and symptoms of heart disease such as chest pain, dizziness, syncope (fainting), heart murmurs, irregular heartbeats, dyspnea (shortness of breath), fatigue, and decreased exercise tolerance [3]. This is information is then supplemented with results

Structural or Functional Abnormality	Resultant Heart Disease
Elevated pressure in the circulatory system against which the heart must pump	Hypertension
Abnormalities in nervous excitation of the heart causing variations in rhythm	Arrhythmia
Blockage in coronary arteries	Ischemic heart disease
Failure of heart valves to open or close normally	Valvular heart disease
Enlarged, thickened and/or stiffened heart muscle	Cardiomyopathy
Structural malformations by birth	Congenital heart disease

Table 1-1 Examples of heart abnormalities and their resultant heart disease.

from laboratory investigations such as blood tests, chest radiography, and resting and exercise electrocardiography. Individuals determined to be at risk or symptomatic are then referred to a cardiologist for further assessment and evaluation to determine the etiology and severity of the disease [3] (Figure 1-3). This is carried out using a case-specific combination of advanced imaging modalities such as transthoracic and stress echocardiography, computed tomography, magnetic resonance imaging, and cardiac catheterization. The cardiologist uses results from these tests to then guide treatment and care.

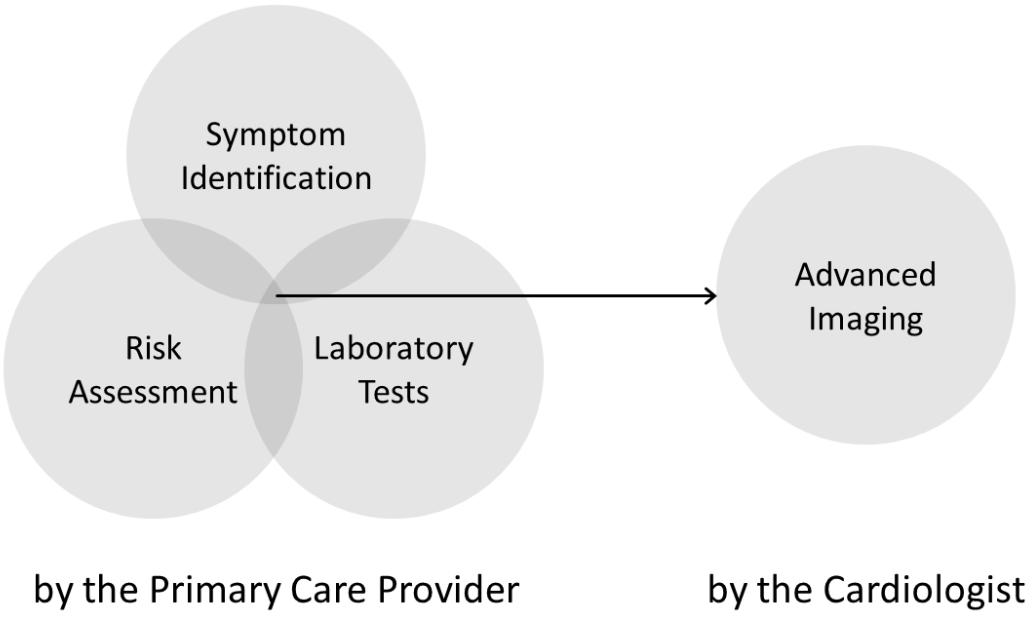

Figure 1-3 Path of care for diagnosing and evaluating heart disease. Individuals determined to be at risk or symptomatic at the point of primary care are referred to the cardiologist for further assessment to determine the etiology and severity of the disease.

1.3 The Need for New Care Delivery Tools

As of 2020, heart disease is the leading cause of death in the United States and nearly 50% of American adults are afflicted with some form of heart disease [4] [5]. Although the past decade has seen a 15% reduction in mortality due to heart disease, this drop is significantly smaller than in previous decades due to increased prevalence of obesity and high blood pressure [6]. Care outcomes are especially poor in individuals who are apparently asymptomatic at the point of primary care, individuals who are misdiagnosed, individuals who do not follow up with a cardiologist or skip a recommended test, and individuals in low resource settings who are unable to access

quality care [6] [7] (Figure 1-4). In addition to concerning mortality trends and missed opportunities in care delivery, the total health expenditure on heart disease is also expected to double to $1.1 trillion by 2035 [4]. Limiting this growing burden of heart disease requires new care-delivery strategies and evidence-based technologies that can provide risk identification, disease diagnosis, and medical evaluation well in advance of the onset of a life-threatening heart disease [7]. The introduction of such technologies and tools will allow to shift the emphasis of healthcare delivery from urgent "sick care" to preventive "well care" [7].

A tool that addresses this need must overcome limitations of existing risk assessment tools and imaging modalities [3] (Table 1-2). It must be usable at the point of

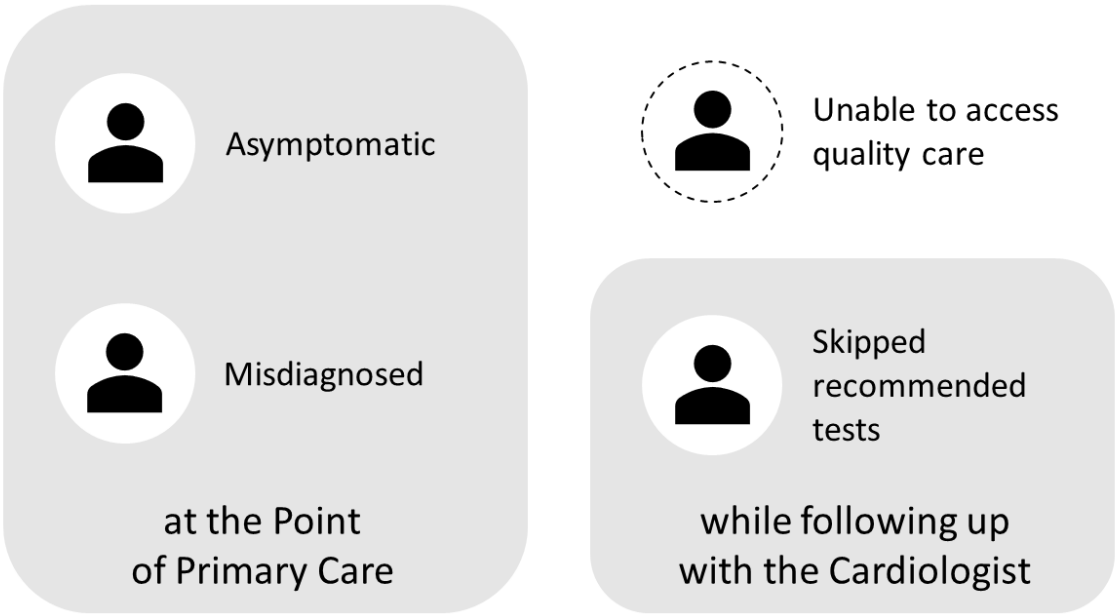

Figure 1-4 Examples of individuals with heart disease for whom care outcomes are poor. Such missed opportunities in care delivery, coupled with increased mortality and healthcare expenditures necessitate the introduction of new tools and technologies for diagnosing and evaluating heart disease.

primary care, must be noninvasive, must not require training and experience to operate, and must be free of inter-operator variability. The diagnostic goal of this tool would be to identify apparently asymptomatic patients at the point of primary care without expert supervision, and the evaluative goal would be to assess heart function without requiring resource-intensive imaging modalities or follow-up visits. In addition, in order to be clinically relevant, this tool must have been developed and validated using real-world data.

Tool / Imaging Modality	**Advantages**	**Limitations**
Blood pressure monitor	Noninvasive, cost effective, available at the point of primary care, requires minimum training for use	High blood pressure is only one of many risk factors for heart disease
Blood test	Highly sensitive to metabolic disturbances in heart disease	Invasive
Auscultation	Noninvasive, available at the point of primary care, can identify structural pathologies even in their presymptomatic phase	Using a stethoscope requires training and expertise
Chest radiography	Noninvasive, useful for initial diagnosis and risk stratification	X-ray findings are usually nonspecific
Electrocardiography	Noninvasive, cost-effective, available at the point of primary care, quick way to detect underlying heart disease	Limited in types of disease that can be diagnosed, high false-positive rate

Echocardiography	Noninvasive, useful for visualizing hemodynamics, can help evaluate disease progression, portable or handheld machines now available at the point of primary care	Requires training and experience to operate, subject to inter-operator variability
Computed tomography / magnetic resonance imaging	Noninvasive, allows for detailed assessment of heart structure and function	Too resource intensive to be used for screening at the point of primary care
Cardiac Catheterization	Helps determine severity of disease and optimal timing for intervention	Highly invasive

Table 1-2 Advantages and limitation of existing risk assessment tools and imaging modalities used for heart disease diagnosis and evaluation.

1.4 The Utility of Phonocardiogram Signals

Computer-aided heart-sound-based tools carry the potential to fulfil this need. Such tools analyze phonocardiograms, which are digital recordings of sounds produced by the heart as it pumps blood [1]. Phonocardiogram signals are collected using microphones placed on the chest that are specially designed to capture low frequency vibrations in heart sounds that cannot be heard through a stethoscope [1]. This reveals characteristics of heart-valve motion, muscle-wall motion and blood-flow dynamics that can be analyzed to identify anatomical and physiological abnormalities in the heart [1]. Phonocardiogram signals can be collected and analyzed in an automated fashion without

expert supervision, which makes them an ideal candidate to form the technological basis of a noninvasive tool that can support healthcare providers in the diagnosis and evaluation heart disease in low-resource settings.

Prior research has demonstrated the utility of phonocardiogram signals (with or without a simultaneously recorded electrocardiogram signal) in establishing the presence of a heart murmur [8], in differentiating between innocent and pathological heart murmurs [9], and in evaluating the severity of a previously identified disease [10] [11]. This is done by extracting temporal or spectral features from the phonocardiogram signal and supplying these as inputs to linear classifiers or artificial neural networks. Although existing studies provide good proof of concept, some have only been primarily validated on pediatric patients [9] [11], and some used completely healthy subjects [10] or subjects without any comorbidities in their control group [8]. Such limitations prevent existing phonocardiogram-based tools from being clinically relevant at the point of primary care for patients with unpredictable medical histories across all age groups.

1.5 Developing a Phonocardiogram-Based System

Presented here is a phonocardiogram-based system that overcomes existing challenges to provide clinically relevant diagnosis and evaluation at the point of primary care (Figure 1-5). This system analyzes simultaneously recorded phonocardiogram and electrocardiogram signals to characterize physiological phenomena of interest. It is capable of both detecting disease in their preclinical phase and evaluating their severity over time. The system has been developed and validated using real-world data collected from a variety of inpatients at the Ronald Reagan University of California Los Angeles Medical Center and the Oregon Health & Science University Hospital. The use of this system at the point of primary care can support healthcare providers in decision making

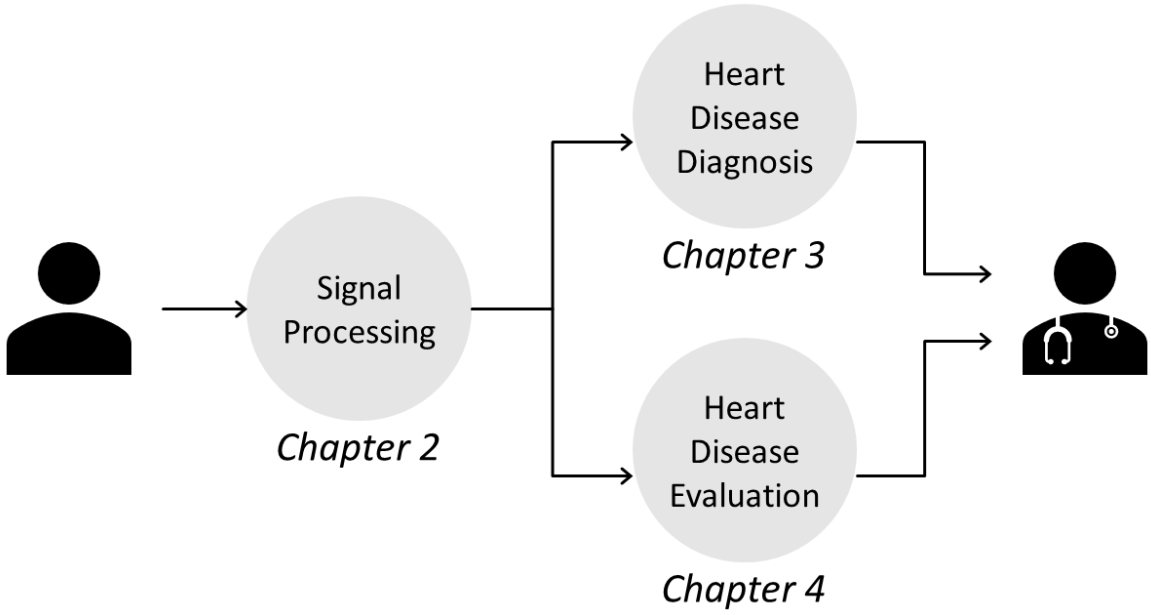

Figure 1-5 Overview of the proposed phonocardiogram-based system and dissertation chapter content.

and allow for better funneling of patients to the cardiologist. This system also shows potential in pre- and post-operative evaluation of patients undergoing cardiac interventions and can also be incorporated in a wearable form factor for day-to-day activity and exercise monitoring.

The design of the proposed system is introduced in Chapter 2 (Phonocardiogram Signal Processing). This includes a description of signal acquisition techniques, challenges in signal processing, and the novel signal processing algorithms designed to address these. Chapter 3 (Diagnosing Heart Disease) describes the utility of the proposed system in diagnosing aortic stenosis in a n=96 subject set. This involves a description of feature extraction and classification algorithms used and the results obtained. Chapter 4 (Evaluating Heart Disease) expands on this discussion and presents the utility of the proposed system in evaluating left ventricular diastolic function in a n=34 subject set. Chapter 5 summarizes this development and proposes ideas for future development.

CHAPTER 2

PHONOCARDIOGRAM SIGNAL PROCESSING

2.1 Signal Acquisition

For the purpose of developing and validating the proposed system, synchronous phonocardiogram and electrocardiogram signals were acquired from hospital inpatients using acoustic sensors and electrodes (Figure 2-1). Each acoustic sensor consisted of an electret microphone housed in an acrylonitrile-butadiene-styrene plastic body with a 0.4mm-thick nitrile membrane at one end. These were placed membrane side down by the provider at each of the four auscultation points on the anterior chest wall: aortic (second intercostal space, right sternal border), pulmonic (second intercostal space, left sternal border), tricuspid (fourth intercostal space, left sternal border) and mitral (fifth intercostal space, left mid-clavicular line) [1]. Locations for sensor placement were

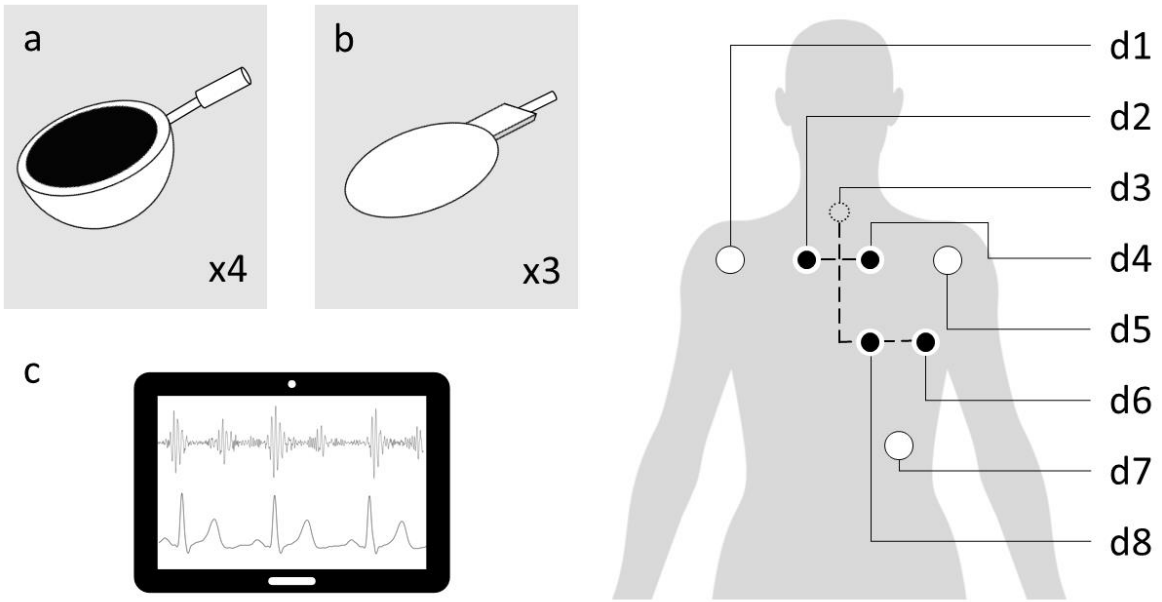

Figure 2-1 An illustration of tools and techniques used in signal acquisition. a) Four acoustic sensors for acquiring phonocardiogram signals. b) Three electrodes for acquiring electrocardiogram signals. c) Computer-based device used to record and store the acquired signals. Locations for sensor and electrode were determined relative to the suprasternal notch (d3). Acoustic sensors were placed at the four auscultation points: aortic (d2), pulmonic (d4), tricuspid (d8), and mitral (d6). The electrocardiography electrodes were placed at the right upper limb (d1), left upper limb (d5), and lower left abdomen (d7).

determined relative to the suprasternal notch and did not require provider intervention. The membrane provided coupling with the chest wall and allowed for the transfer of heart sound signals into the sensor chamber for measurement by the microphone. Three electrocardiography electrodes were placed proximally on the two upper limbs and lower left abdomen. These measured the cardiac action potential in an augmented-unipolar-limb-lead configuration [1]. The acoustic sensors and electrodes were connected to a computer-based device [12] and phonocardiogram and electrocardiogram signals were acquired at sample rates of 512 and 300 Hz, respectively (Figure 2-2). Signal acquisition

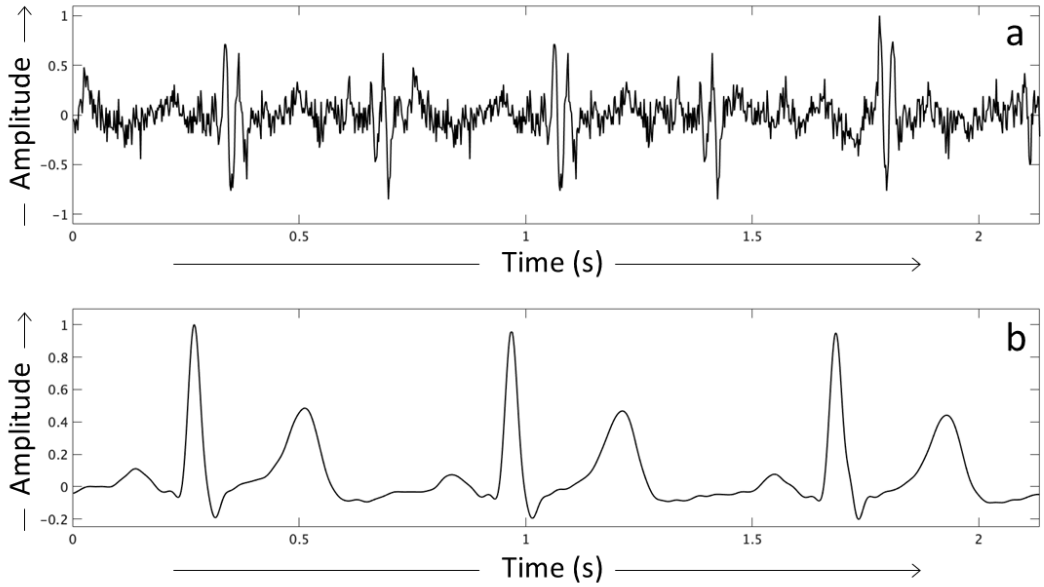

Figure 2-2 Examples of unprocessed phonocardiogram (a) and electrocardiogram (b) signal waveforms acquired from each subject.

was designed to last for 5 to 7 minutes (depending on the hospital schedule) during which subjects were asked to relax and refrain from motion or speaking if possible. The acquired signals were stored in 10-second-long intervals and were later imported into Matlab (MathWorks, MA, USA) for offline exploration and analysis.

2.2 Challenges in Signal Processing

Analyzing these phonocardiogram signals to extract valuable heart sound information required overcoming challenges of variable signal quality. The first source of this variability was the non-controlled and fast-paced nature of the hospital environment. This led to occasional physiological, environmental, and instrumental noise artifacts in

the phonocardiogram signal, including those from subject speech and motion, bystander speech, hospital alarms and announcements, and poor coupling between the acoustic sensors and chest. The second source of variability was the dynamic nature of subject physiology. This included variable heart rates, variable heart structures, and unique pathophysiology that only manifested in certain heartbeats. The challenges posed by variable signal quality were addressed by creating a novel signal processing algorithm that allowed for the identification of noise-free, high-quality, and reliable heartbeats. This was a three-step process (Figure 2-3). The first step involved filtering and noise subtraction to obtain phonocardiogram signals of qualitatively higher audio fidelity than raw signals. The second step involved segmentation algorithms that divided the clean

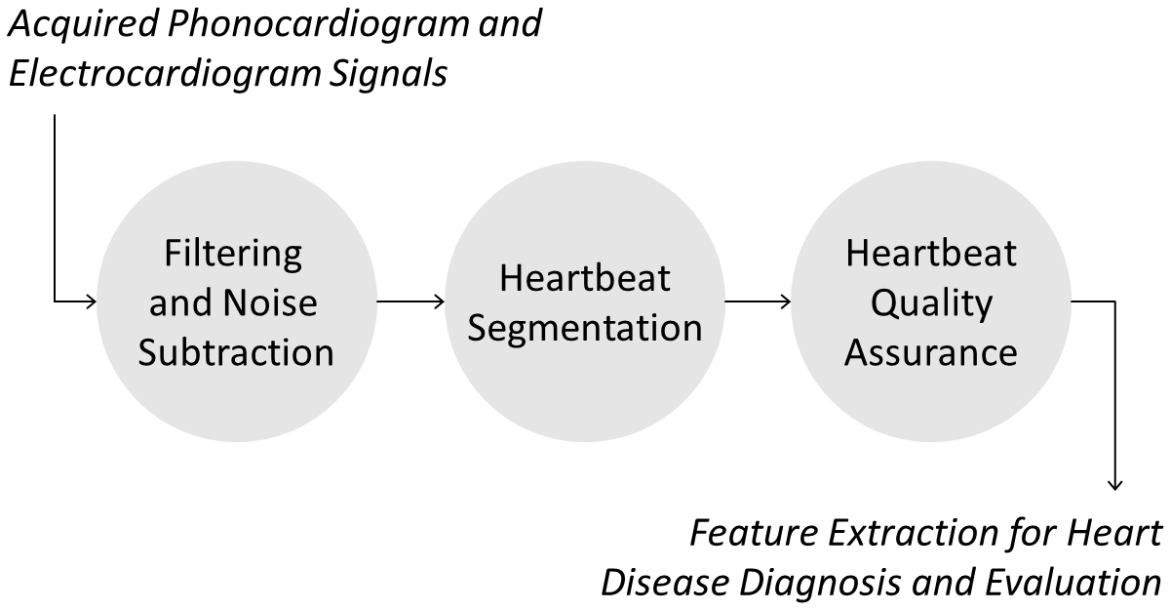

Figure 2-3 An overview of the signal processing algorithm created to address challenges posed by variable signal quality. Feature extraction algorithms defined in Chapters 3 and 4 use these processed phonocardiogram signals for heart disease diagnosis and evaluation.

phonocardiogram signal from step one into individual heartbeats. And the third step consisted of a quality assurance algorithm designed to identify high-quality heartbeats even in severely afflicted subjects or those with variable heart rate. The entire phonocardiogram signal processing algorithm operated in a fully automated fashion.

2.3 Filtering and Noise Subtraction

The process of designing a filtering and noise subtraction algorithm for the raw phonocardiogram signal (originally sampled at 512 Hz) began with a visualization of its frequency-domain representation between 1 and 256 Hz (Figure 2-4). The discrete Fourier transform of short signal segments chosen at random showed recurring low-to-mid frequency range patterns matching closely with the spectrum of heart sounds [1]. The raw signal was subsequently filtered using a fourth-order Butterworth band-pass filter with cutoff frequencies of 25 and 140 Hz (Figure 2-5). These cutoff frequencies were chosen empirically to retain the maximum amount of heart sound information while removing most low and high-frequency noise artifacts.

The remaining noise artifacts overlapping with the mid-frequency heart sound signal spectrum were removed using a spectral noise subtraction technique commonly used in speech processing [13]. This technique involved estimating the noise spectrum during brief pauses in heart sound activity and then subtracting this estimate from the entire signal's spectrum to obtain a clean heart sound signal (Figure 2-6).

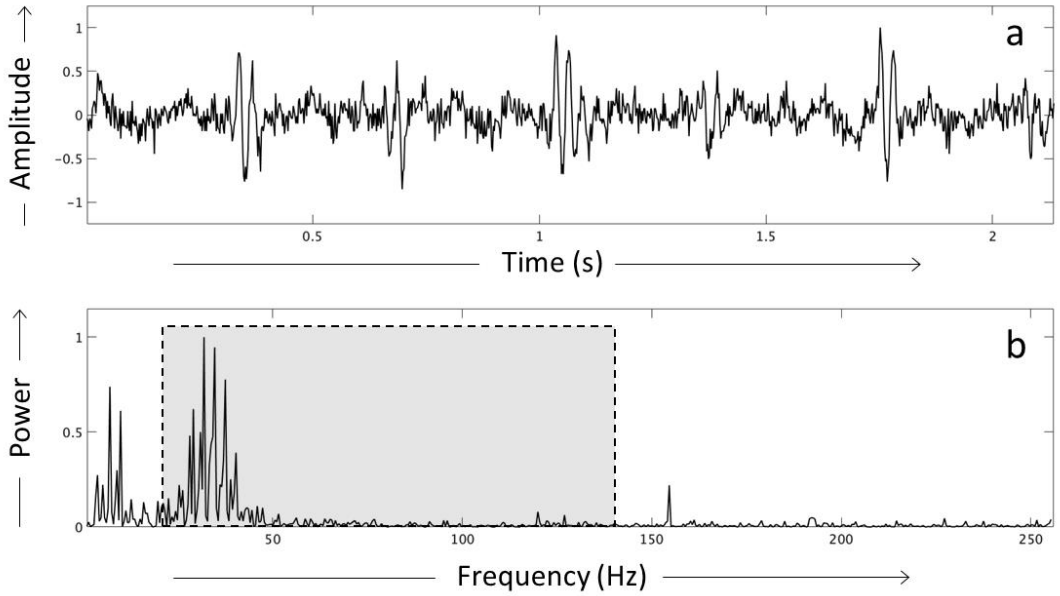

Figure 2-4 Time (a) and frequency-domain (b) representation of a raw phonocardiogram signal segment chosen at random. a) The time domain representation shows normalized signal amplitude for a 2-second-long signal segment. b) The frequency domain representation shows normalized power for this segment in the frequency range 1 to 256 Hz. An analysis of multiple segments revealed similar recurring patterns in the 25 to 140 Hz range (shaded box) matching closely with the spectrum of heart sounds. These frequencies were therefore chosen to design a band-pass filter to extract this heart sound information.

Regions of the phonocardiogram signal corresponding to pauses in heart sound activity were identified by visualizing the histogram distribution of the signal envelope in each 10-second phonocardiogram recording. For this purpose, a fourth-order Butterworth low-pass filter with a cutoff frequency of 38 Hz was applied to the phonocardiogram signal. The signal envelope obtained as a result was then divided into 93 millisecond-long frames with 31 millisecond (33%) overlaps between adjacent frames. The frame and overlap lengths here were empirically determined to provide the best noise subtraction. Next, the amplitude distribution for the signal envelope was obtained

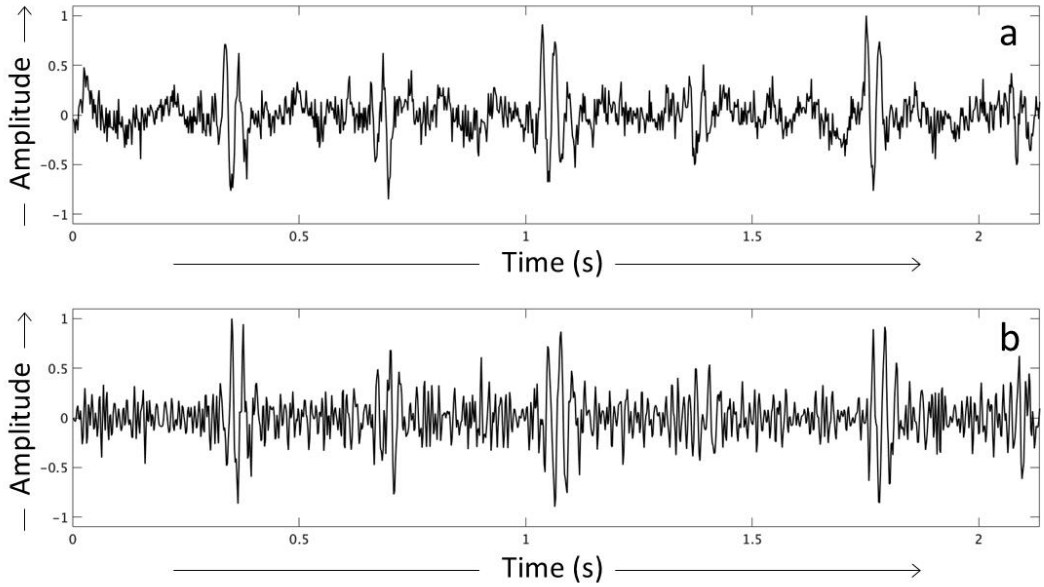

Figure 2-5 Illustration of a phonocardiogram signal segment before (a) and after (b) the application of a fourth-order Butterworth band-pass filter with cutoff frequencies of 25 and 140 Hz to remove most low and high-frequency noise artifacts. The plots show normalized signal amplitudes for the 2-second-long phonocardiogram signal segment.

by arranging the root-mean-square amplitude values of individual frames in increasing order. This amplitude distribution had a roughly bimodal shape with one peak for lower amplitude values corresponding to pauses in heart sound activity and another peak for higher amplitude values corresponding to physiological and pathological heart sounds. Frames in the first peak of the amplitude distribution with amplitude values between the 60^{th} to 99^{th} percentile of this peak were then selected to estimate the noise spectrum, as these were observed to provide the best denoising during algorithm development (Figure 2-7). The individual frequency spectra for the selected frames were calculated using a discrete Fourier transform, and these spectra were then averaged to approximate one overall noise spectrum for that recording. This average noise spectrum was then

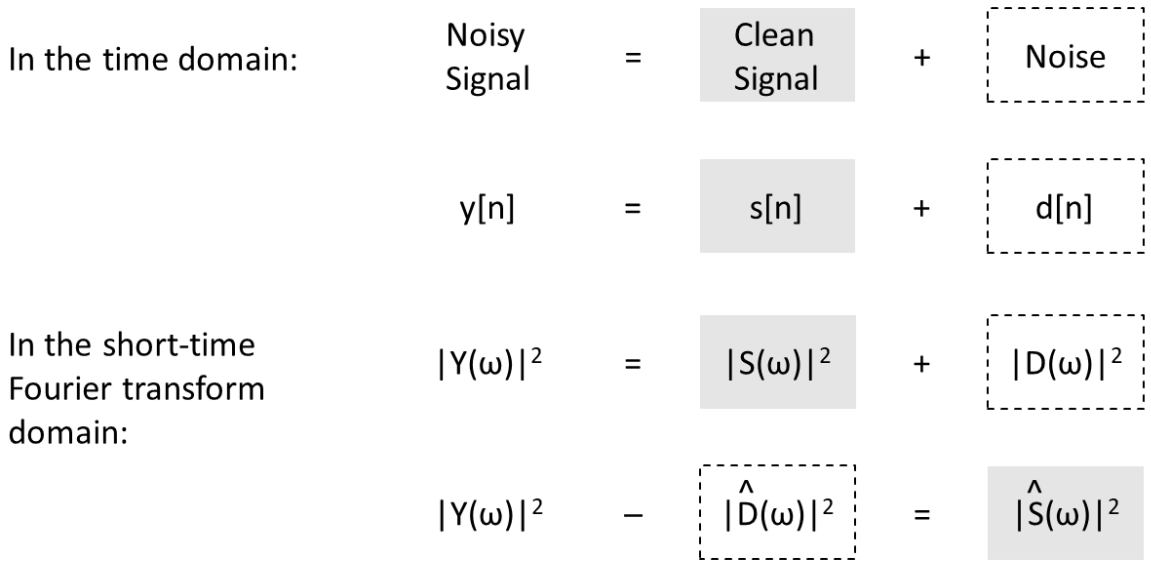

Figure 2-6 Visual representation of the spectral noise subtraction technique used to obtain a clean heart sound signal. The noisy phonocardiogram signal (y[n]) is assumed to be composed of the clean signal (s[n]) degraded by statistically independent noise (d[n]). This relation also holds true in the short-time Fourier transform domain for the respective power spectra of these signals: $|Y(\omega)|^2$, $|S(\omega)|^2$, and $|D(\omega)|^2$. Here, the clean signal spectrum ($|\hat{S}(\omega)|^2$) is obtained by subtracting the average noise estimate spectrum ($|\hat{D}(\omega)|^2$) from the noisy signal spectrum on a frame-by-frame basis. The inverse Fourier transforms of clean signals in individual frames are then added up to recover the clean heart sound signal in the time domain.

subtracted from individual discrete Fourier transforms of all available frames, including those belonging to heart sound activity. The resulting frequency spectrum for each frame was now noise-free, and its corresponding time-domain signal was recovered by performing an inverse Fourier transform. Noise-free signals in each frame were then added together while accounting for the original 33% overlap to reconstruct the phonocardiogram signal for the entire 10-second recording. Finally, the same band-pass filter as before with cutoff frequencies of 25 and 140 Hz was reapplied to the resulting

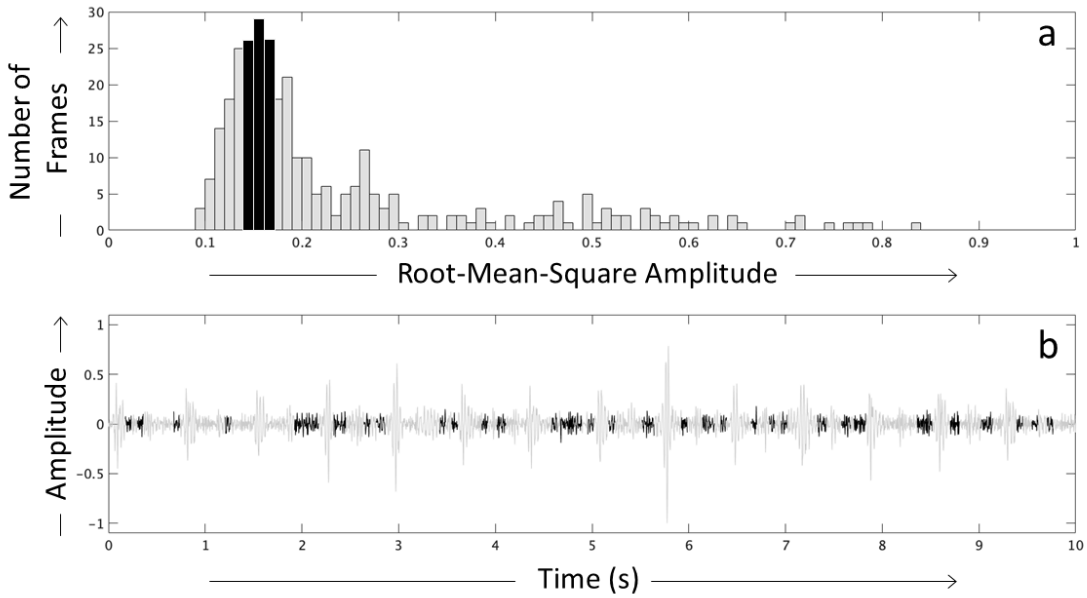

Figure 2-7 Identifying frames corresponding to pauses in heart sound activity for the purpose of noise subtraction. a) Amplitude distribution plot for 93 millisecond-long frames in the signal envelope of a 10-second long recording. This amplitude distribution shows a roughly bimodal shape with one peak for lower amplitude values (centered around 0.15 on the x-axis) corresponding to pauses in heart sound activity, and one peak for high amplitudes (centered around 0.27 on the x-axis) corresponding to heart sound. Frames in the first peak with amplitude values between the 60th to 99th percentile of this peak are highlighted in black and were chosen to estimate the noise spectrum. b) Normalized signal amplitude for the corresponding 10-second phonocardiogram recording. Frames that fell in the 60th to 99th percentile of the peak above and were used to estimate the noise spectrum are marked in black.

waveform to obtain a clean phonocardiogram signal. The signal-to-noise ratio for this denoised phonocardiogram signal was found to be significantly higher than the raw signal (Figure 2-8).

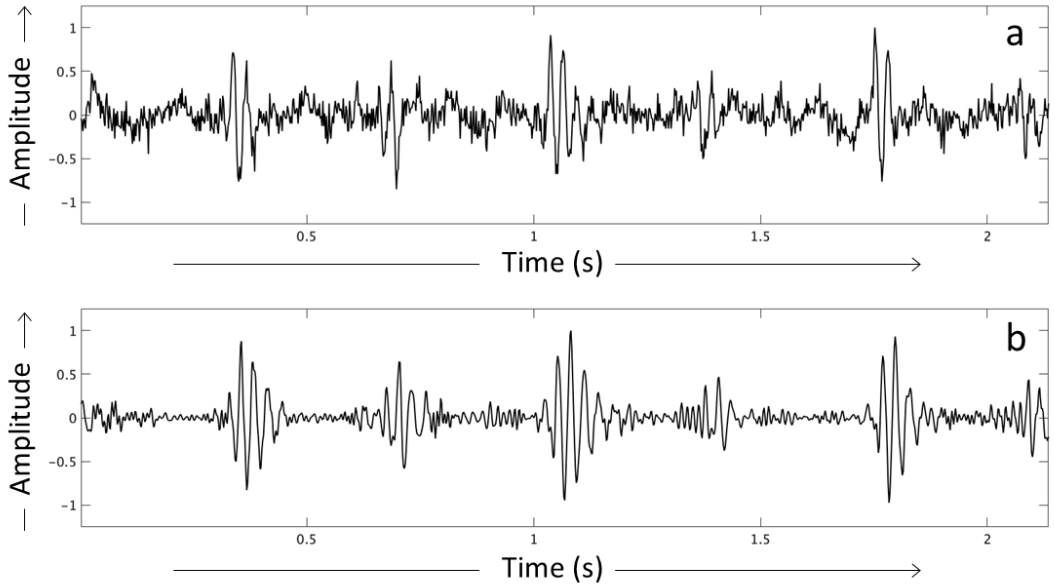

Figure 2-8 Illustration of a phonocardiogram signal segment before (a) and after (b) filtering and noise subtraction. The plots show normalized signal amplitude for a 2-second-long phonocardiogram signal segment. a) The raw phonocardiogram signal had a low signal-to-noise ratio due to physiological, environmental, and instrumental noise. b) The denoised phonocardiogram signal showed clearly defined periodic heart-sound waveforms and was of qualitatively higher audio fidelity than the raw signal.

2.4 Heartbeat Segmentation

After obtaining a filtered and denoised signal, the next step involved identifying the start and end times of individual heartbeats in the phonocardiogram signal. This was done using the electrocardiogram signal as reference. The onset of the R wave in each cardiac cycle of the electrocardiogram signal was regarded as the transition point between the end of one heartbeat and start of the next one. This point corresponded to the start of the S1 heart sound in the phonocardiogram signal [1]. To identify this point, a

fourth-order Butterworth band-pass filter with cutoff frequencies of 1 and 30 Hz was applied to the electrocardiogram signal (originally sampled at 300 Hz). The cutoff frequencies here were chosen to reject 0.5 Hz baseline-drift noise from incorrect electrode attachment or subject motion, and 60 Hz noise from power-line interference [14]. The resulting signal represented the characteristic recurring P-QRS-T pattern of a cardiac action potential [1]. While R waves were expected to show the largest signal amplitude, signal peaks were seen to be equally likely to correspond to either R or T waves. Although these were of similar amplitudes, the R peaks were observed to be sharper than the T peaks. Multiplying the signal with its derivative therefore helped emphasize R peaks, thereby allowing for their identification in the electrocardiogram signal (Figure 2-9). Outlier peaks that were much larger (>5x) or much smaller (<0.5x) than median peak height were rejected as these were most likely due to noise or abnormalities in cardiac electrophysiology [1]. Peaks that were within 0.25 seconds of adjacent peaks were also rejected to account for variations in heart rate. The exclusion of occasional outlier peaks did not pose a challenge to further signal processing. The onset of each R wave in each remaining peak was determined by searching backwards from the peak to the time point corresponding to 50% peak height. The electrocardiogram signal between two consecutive onset points was then identified as one cardiac cycle, and the corresponding phonocardiogram signal was therefore identified as one heartbeat (Figure 2-10).

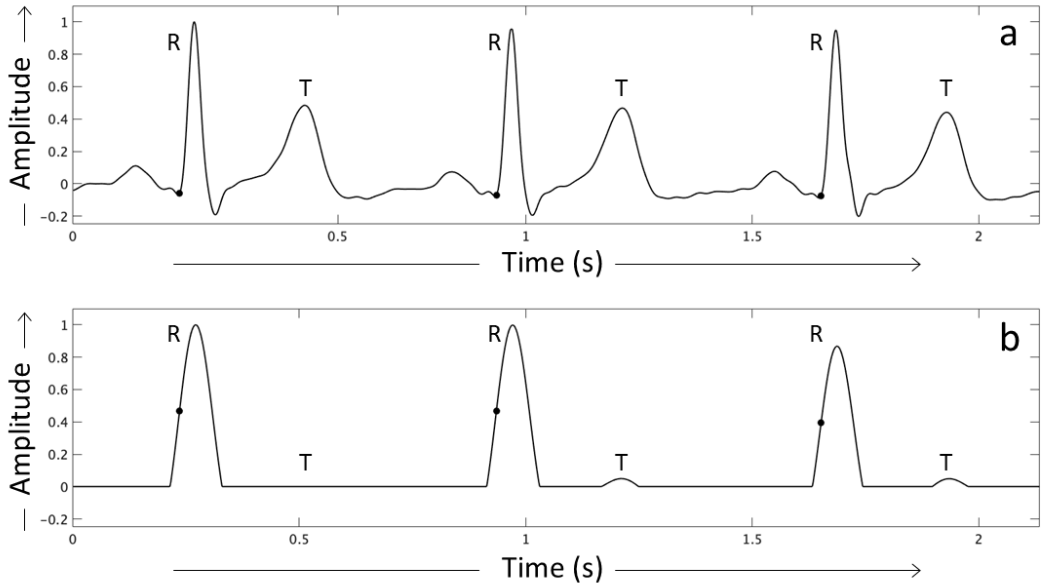

Figure 2-9 Determining the onset of R waves for segmenting electrocardiogram signals. a) The electrocardiogram signal shows normalized signal amplitude for a 2-second-long filtered signal segment. Signal peaks were equally likely to correspond to either R or T waves. b) Multiplying the signal with its derivative helped emphasize R peaks as these were sharper than T peaks. The onset of the R wave was determined by searching backwards for the time point corresponding to 50% peak height, marked as black dots. The electrocardiogram signal in (a) between two consecutive black dots was then identified as one cardiac cycle.

Once individual heartbeats were identified in the phonocardiogram signal, the next step involved identifying start and end times for the two heart sounds, S1 and S2. This was done by utilizing the short-term periodicity of the cardiac cycle which existed even in severely afflicted cases. To identify the first heart sound, the denoised but unsegmented phonocardiogram signal was low-pass filtered using a fourth-order Butterworth filter with a cutoff frequency of 10 Hz. The signal envelope hence obtained showed peaks corresponding to the recurring S1 and S2 heart sounds. Using the

previously acquired knowledge of endpoints for individual heartbeats, this signal envelope was then divided into two-heartbeat-long frames with an overlap of one heartbeat among adjacent frames. A cross correlation was performed for each frame in this filtered signal envelope with a comb function of value zero at all points except t=0 and t=T (where T was the time period of the first of the two heartbeats). The location of impulses in this function were expected to be close to the onset of R waves in the electrocardiogram signal, and therefore the onset of the S1 heart sound in the phonocardiogram signal. The first most prominent peak in the cross-correlation time

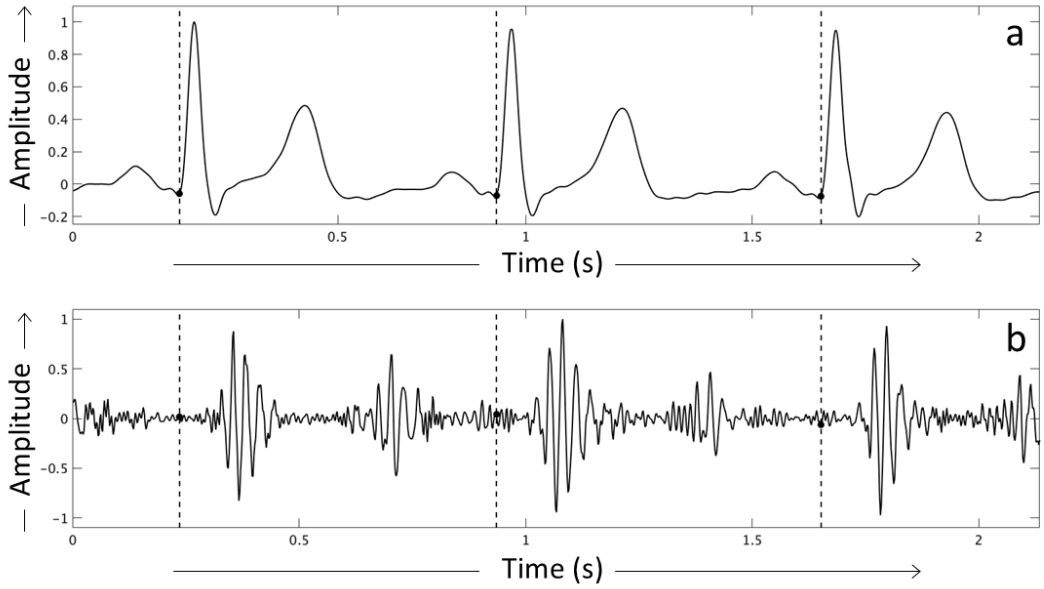

Figure 2-10 Using the electrocardiogram signal as reference to segment the phonocardiogram signal into individual heartbeats. a) The electrocardiogram signal showing normalized amplitude for a 2-second-long filtered signal segment. Time points corresponding to the start and end of individual cardiac cycles are marked with vertical dotted lines. b) The corresponding phonocardiogram signal segment showing normalized signal amplitude. The phonocardiogram signal between two vertical dotted lines was identified as one heartbeat.

series was therefore expected to occur when the first comb function impulse aligned perfectly with the S1 peak of the first heartbeat. This helped determine the location of the first S1 peak in this frame. The S1 peak belonging to the second heartbeat was subsequently determined to occur T seconds after the first S1 peak. Once both S1 peak locations were known, the corresponding start and end times for the S1 heart sounds were determined by searching backwards and forwards from the peak to the time point corresponding to 60% peak height (Figure 2-11). The one frame overlaps between consecutive frames allowed for each beat (except the first and last) to be processed twice to increase detection rate for heart sounds. Start times for individual heartbeats were also updated to coincide with start times for S1 heart sounds instead of the previously used points corresponding to the onset of the R wave in the electrocardiogram signal.

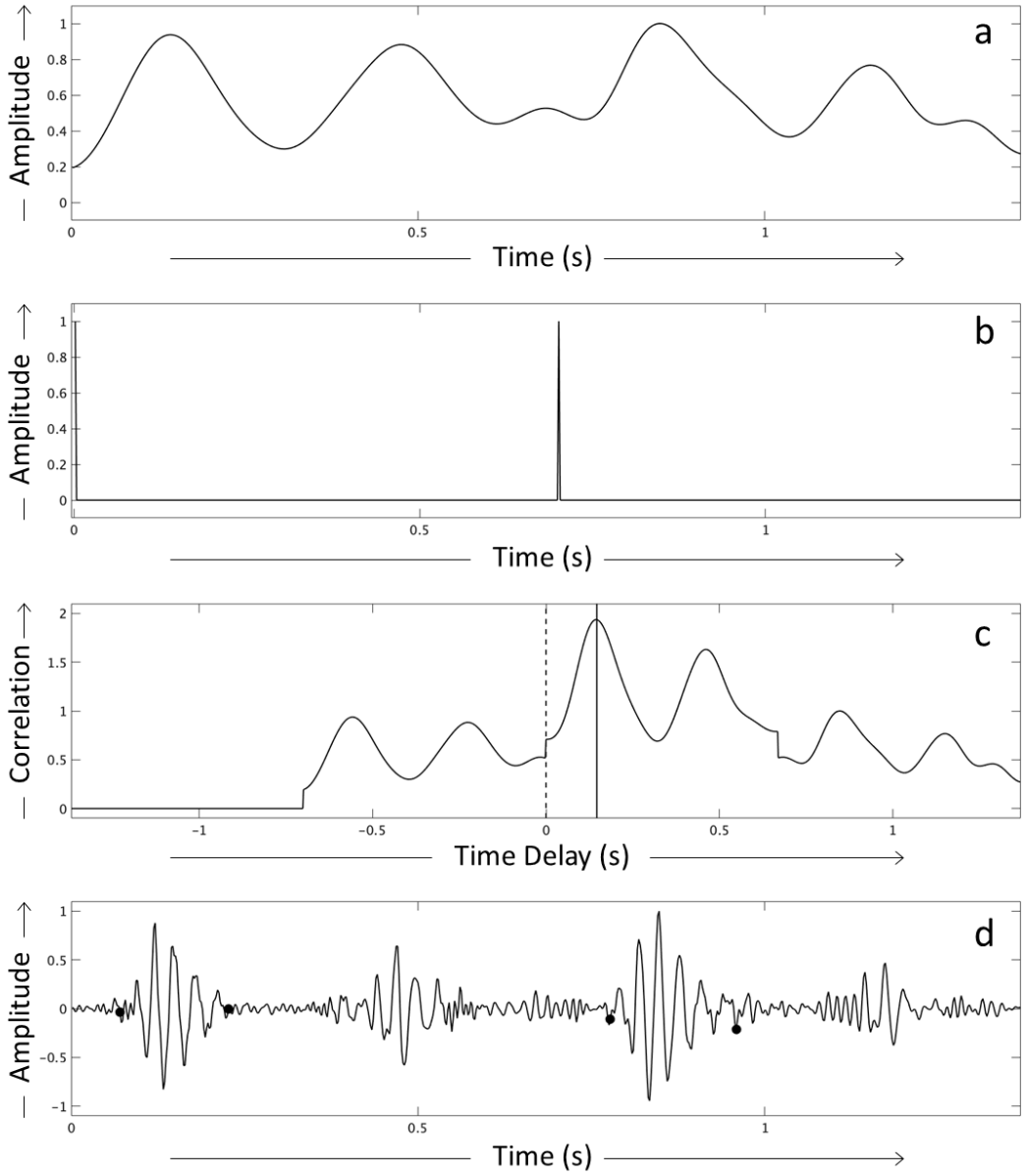

Figure 2-11 Identifying start and end times of S1 heart sound in each two-heartbeat-long frame. a) Signal envelope calculated using a cutoff frequency of 10 Hz, showing normalized amplitude for the denoised but unsegmented phonocardiogram signal in each frame. b) The comb function showing two impulses at t=0 and t=T seconds (where T was the time period of the first heartbeat). c) The cross-correlation time series showing the point of zero time delay as a vertical dotted line, and the point of the first prominent peak as a vertical solid line. The time delay between these two points represented the location of the S1 peak relative to the start of the heartbeat containing it. The location of the S1 peak for the

second heartbeat was subsequently determined to be T seconds after the first. d) Phonocardiogram signal showing points corresponding to the start and end times of the S1 heart sounds, determined by searching for signal amplitudes equal to 60% of peak height on either side of the peak.

The same method was used to identify the second heart sound, however this time the signal envelope was computed using a cutoff frequency of 15 Hz. This value was empirically chosen to preserve a greater resolution of the original signal and gave prominent correlation peaks allowing for the identification of the start and end times for the S2 heart sound. For this purpose, a cross correlation was performed for each frame in the new filtered signal envelop with the same comb function as above. Previous signal analysis experiments revealed that S2 peaks were found within 0.2T and 0.55T seconds of the S1 peak. Therefore, the peak in the cross-correlation time series occurring in this time interval after the first most prominent peak was expected to occur when the first comb function impulse aligned perfectly with the S2 peak of the first heartbeat. The S2 of the second heartbeat, as well as start and end times for S2 heart sounds were determined in the same manner as above (Figure 2-12). Once the endpoints for the two heart sounds were established in each heartbeat, the phonocardiogram signal between the of S1 and start of S2 was identified as the systolic interval, and that between the end of S2 and start of S1 of the next heartbeat was identified as the diastolic interval (Figure 2-13). This segmented denoised signal was then used as reference to mark corresponding endpoints in the raw phonocardiogram signal.

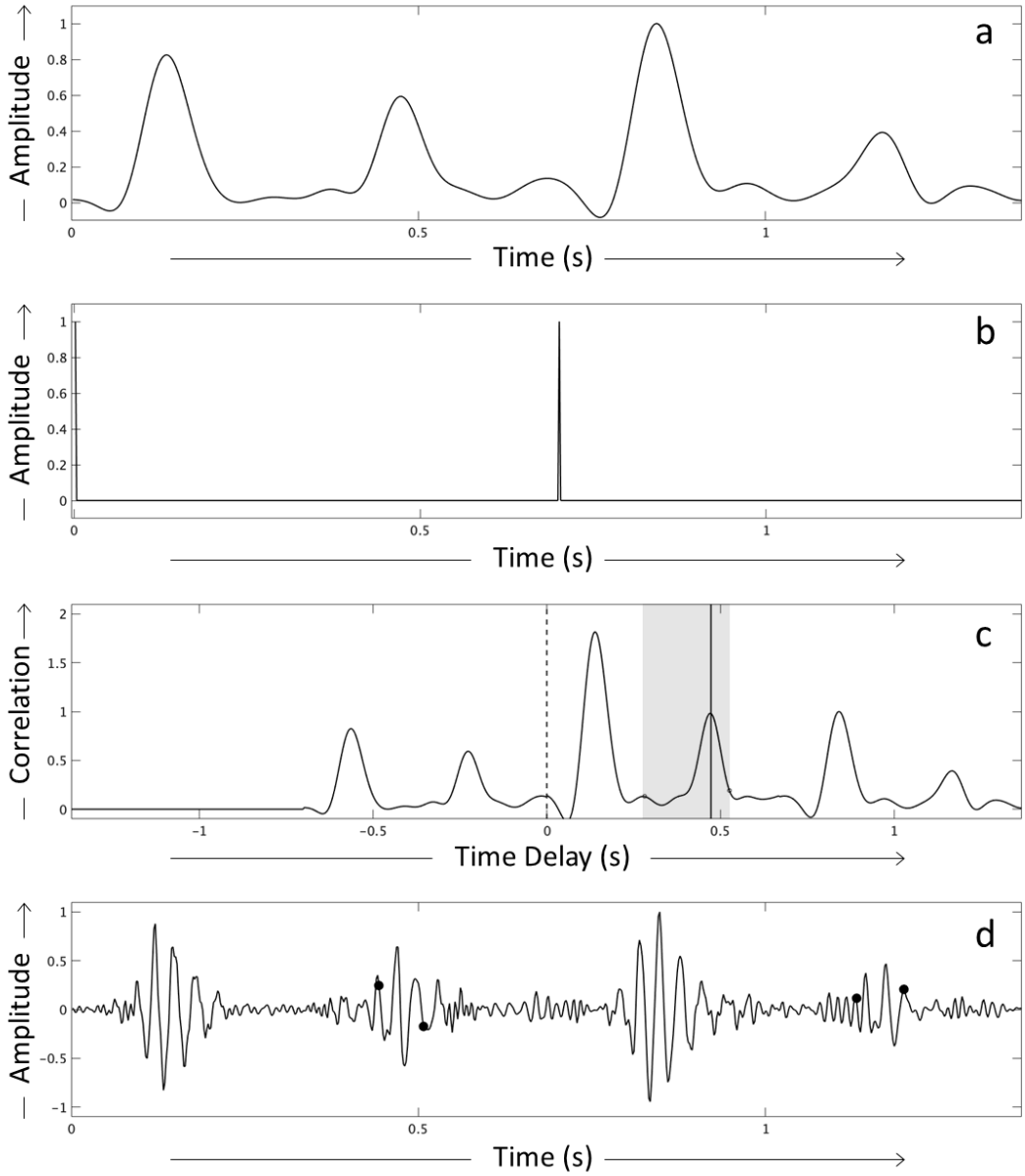

Figure 2-12 Identifying start and end times of S2 heart sound in each two-heartbeat-long frame. a) Signal envelope calculated using a cutoff frequency of 15 Hz, showing normalized amplitude for the denoised but unsegmented phonocardiogram signal in each frame. b) The comb function showing two impulses at t=0 and t=T seconds (where T was the time period of the first heartbeat). c) The cross-correlation time series showing the point of zero time delay as a vertical dotted line, the period of search for the second most prominent peak (0.2T to 0.55T) in the shaded box, and the point of the second most prominent peak as a vertical solid line. The time delay between the two vertical lines represented the location of

the S2 peak relative to the start of the heartbeat containing it. The location of the S2 peak for the second heartbeat was subsequently determined to be T seconds after the first. d) Phonocardiogram signal showing points corresponding to the start and end times of the S2 heart sounds, determined by searching for signal amplitudes equal to 60% of peak height on either side of the peak.

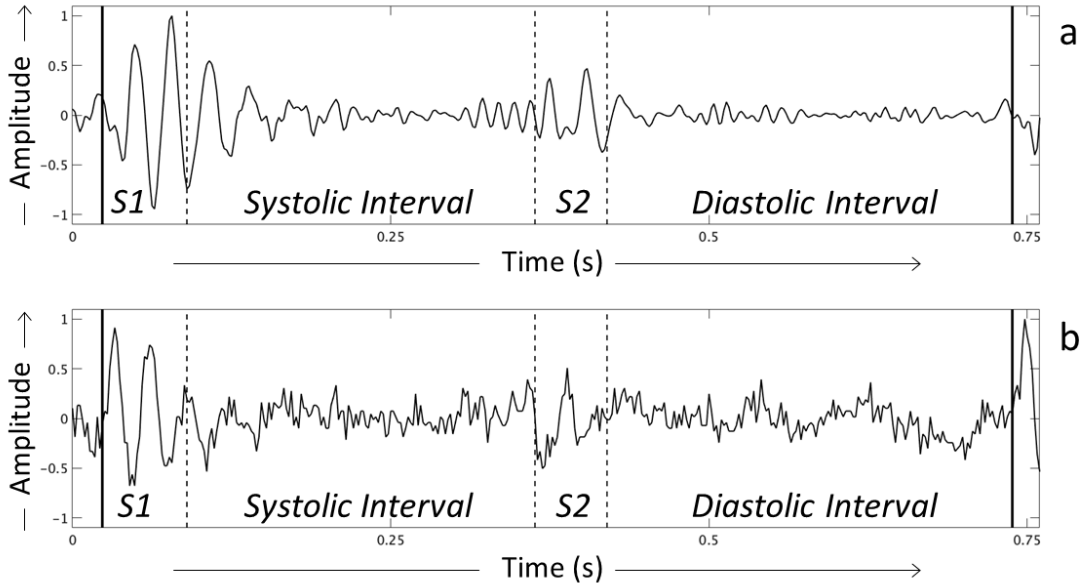

Figure 2-13 Example of a fully segmented heartbeat. a) The normalized signal amplitude for the denoised phonocardiogram signal belonging to one heartbeat, showing successfully identified S1 and S2 heart sounds along with the systolic and diastolic intervals between them. b) Normalized amplitude for the raw phonocardiogram signal for the same heartbeat, also showing S1, systolic interval, S2, and diastolic interval. Although the heartbeat segmentation algorithm used denoised phonocardiogram signals, marking the corresponding endpoints in the raw signal allowed for the use of both type of signals in the feature extraction process. Solid vertical lines represent start and end times for the heartbeat, and dotted vertical lines represent start and end times for S1 and S2 heart sounds.

2.5 Heartbeat Quality Assurance

Not all heartbeats in the resulting dataset were perfectly segmented due to weak signal quality. For example, heartbeats in subjects with variable heart rates occasionally had incorrectly identified endpoints. Heartbeats in subjects with variable heart structure and pathophysiology occasionally had missing or misidentified S1 or S2 sounds. There were also a few heartbeats that were still plagued with noise due to poor sensor coupling. A subset of high-quality heartbeats was therefore created for diagnostic and evaluative applications where the entire dataset of heartbeats was not necessary. A heartbeat was identified as a quality heartbeat if its signal: (1) had a heartbeat duration within ± 20% of the median beat duration for the subject, (2) had both S1 and S2 successfully identified, and (3) had systolic and diastolic intervals free of signal excursions greater than 50% height of S1 or S2. Although segmentation was performed on the denoised phonocardiogram signal, knowledge of heart sound endpoints in time were also used to segment the raw phonocardiogram signal for applications requiring analysis of heart sound acquired as-is. The feature extraction process in each of the diagnostic and evaluative applications was therefore designed to utilize a case-specific selection of either raw or denoised phonocardiogram signals belonging to either all or exclusively quality heartbeats.

CHAPTER 3

DIAGNOSING HEART DISEASE

3.1 Goal: Diagnosing Aortic Stenosis

Two criteria were set forward while searching for a disease to validate the diagnostic capability of the proposed phonocardiogram-based system: first, this disease must have a large population of individuals who are apparently asymptomatic at the point of primary care, and second, diagnosing this disease early must provide a considerable improvement in the patient outcomes.

A disease that satisfied both the above criteria was aortic stenosis, which is the most prevalent valvular heart disease in the United States [4]. In this disease, the fibrous opening of the aortic valve becomes narrow, which obstructs the flow of blood from the left ventricle to the rest of the body [1] (Figure 3-1). In the early stages, the left ventricle

muscle increases in size and develops high muscle-wall tension to compensate for the increased workload. This prevents significant abnormalities in circulatory function and the individual continues to believe that they are free of any serious heart disease. However, over time, this compensation reaches a critical limit beyond which the left ventricle is unable to keep up with the increased demand [1]. At this point, blood begins to back up in the left atrium and lungs, and the overall pumping ability of the heart decreases, eventually causing systolic heart failure. Aortic valve replacement surgery is the only treatment in such severe cases of aortic stenosis [15].

Around half the individuals with severe aortic stenosis are apparently asymptomatic at the point of primary care [15]. The care provider is therefore unable to

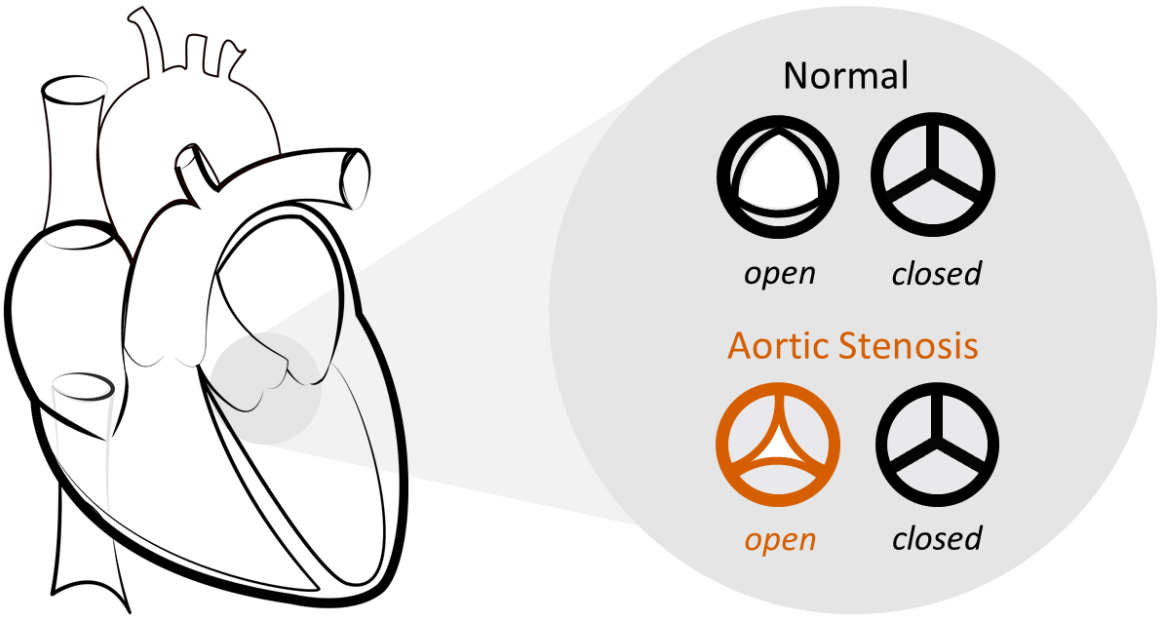

Figure 3-1 Transverse views of normal and stenosed aortic valves. While the normal valve opens and closes fully, the stenosed valve does not open enough, which restricts blood flow from the left ventricle to the rest of the body.

diagnose them, and they do not receive any life-saving surgical intervention. As a result, 70% of asymptomatic individuals end up experiencing sudden death [15]. Prior studies have shown that timely intervention in such individuals is closely associated with increased chances of survival [16]. Early diagnosis of this disease at the point of primary care using the proposed phonocardiogram-based system can therefore have a live-saving impact on these individuals.

3.2 Subject Population

The phonocardiogram and electrocardiogram signals used to validate analytical methods for this purpose were collected after obtaining informed consent from 96 adult inpatients at the Ronald Reagan University of California Los Angeles (UCLA) Medical Center (Los Angeles, CA) between March 2016 and September 2017. This clinical study was approved by the UCLA Office of the Human Research Protection Program (Study Identifier: 14-000670). The subjects were males and females between 19 and 95 years of age (mean age of 57±18 years), between 40 and 116 kg in weight (mean weight of 79±17 kg), and exhibited one or more of 81 types of cardiac and non-cardiac afflicted conditions in their medical history. Signal acquisition lasted between 1 to 16 minutes per subject (mean duration of 7±3 minutes). Out of the 96 subjects, 12 were diagnosed as having aortic stenosis by a medical sonographer using echocardiography (Table 3-1), and these diagnoses were independently confirmed through auscultation by a physician. The availability of this real-world data with reliable ground-truth diagnoses established aortic

stenosis as a valid diagnostic goal for demonstrating the potential of the proposed phonocardiogram-based tool.

Subject Population	**Subject Count**	**Age (years)**	**Weight (kg)**
All Subjects	96	Between 19 to 95 (mean 57±18)	Between 40 to 116 (mean 79±17)
Aortic Stenosis Subjects	12	Between 24 to 95 (mean 68±21)	Between 55 to 97 (mean 74±14)
Non-Aortic-Stenosis Subjects	84	Between 19 to 91 (mean 55±17)	Between 40 to 116 (mean 79±17)

Table 3-1 Subject demographics for aortic stenosis and non-aortic-stenosis subject subgroups.

3.3 Feature Extraction

Phonocardiogram signal processing for diagnosing aortic stenosis relied on the identification of systolic ejection murmurs (Figure 3-2). These murmurs are pathological rumble sounds heard during systole and often indicate abnormalities in heart anatomy or physiology. However, systolic murmurs are also seen in other valvular heart disease such as mitral regurgitation or pulmonic stenosis, in congenital heart disease such as patent ductus arteriosus, in atrial and ventricular septal defects, and in hypertrophic

cardiomyopathy [3]. Therefore, the challenge in signal processing was to identify those systolic murmurs unique to aortic stenosis subjects. This motivated the development of a phonocardiogram feature extraction process that leveraged the location, quality, timing, and intensity of such murmurs.

For this purpose, the filtering, noise subtraction, heartbeat segmentation, and heartbeat quality assurance algorithms described in Chapter 2 were applied to phonocardiogram signals acquired from the n=96 subject set. Signals recorded at the aortic auscultation point were chosen for this analysis due to the proximity of this site to the stenosed aortic valve, allowing for the recording of minimally attenuated broadband

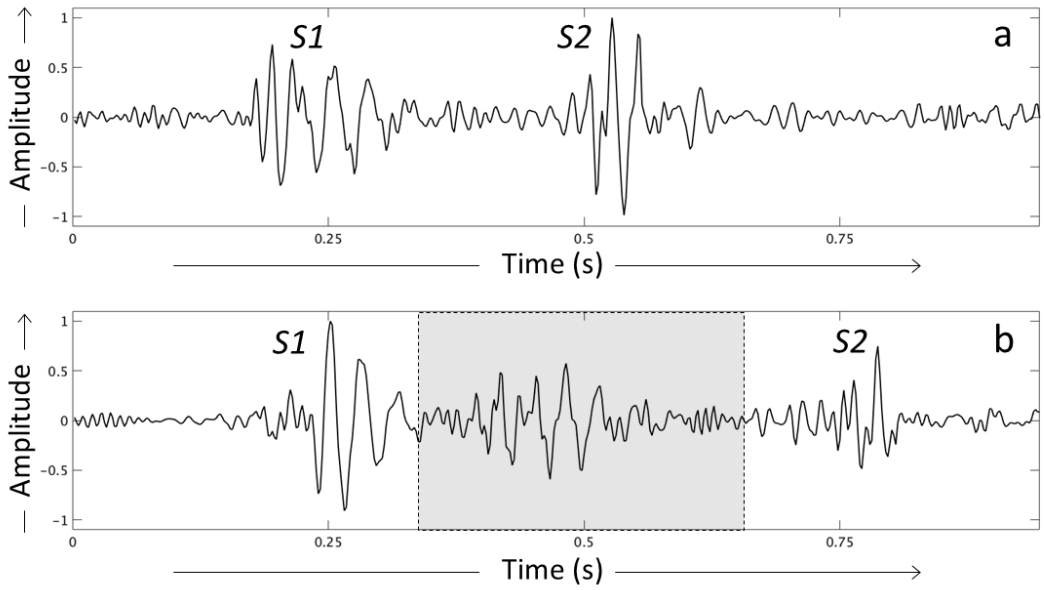

Figure 3-2 Example of systolic murmurs seen in subjects with aortic stenosis. a) Normalized signal amplitude for the phonocardiogram signals belonging to one heartbeat of a non-aortic-stenosis subject. b) Normalized signal amplitude for the phonocardiogram signals belonging to one heartbeat of a subject with aortic stenosis showing a systolic murmur (shaded box).

systolic murmurs. The denoised version of these signals was chosen over the raw version because these were free of any background noise artifacts that could be mistaken as murmurs. Only high-quality heartbeats were included in the analysis dataset because these had reliable markers for the start and end times of systolic intervals. The final heart-sound dataset had 2 to 484 eligible heartbeats per subject (mean beat-count of 127±121 beats).

All subjects with systolic-murmur-inducing conditions were expected to show correspondingly high phonocardiogram signal amplitudes during systole. However, only those subjects that had systolic murmurs due to aortic stenosis were expected to also show elevated levels of high-frequency systolic content [3]. In these subjects, this high-frequency trend was caused by turbulent blood flow through the stenosed aortic valve during systole as a result of the high-pressure gradient between the left ventricle and aorta [1]. While an amplitude-based feature measure systolic interval signal amplitude to detect the presence of systolic murmurs regardless of their physiological origin, a frequency-based feature measured levels of high-frequency systolic content to identify systolic murmurs uniquely seen in aortic stenosis subjects. These features were computed as follows:

1. **Extract the systolic signal segment, d_{sys}, from each heartbeat**: Each heartbeat in the heart-sound dataset contained a well-defined systolic interval. However, some systolic murmurs were known to blend in with S1 or S2 [3]. To take all types of systolic murmurs into account, the phonocardiogram signal segment used for

feature extraction included the second half of S1, full systolic interval, and the first half of S2 (Figure 3-3). A fourth-order Butterworth band-pass filter with cutoff frequencies of 38 and 154 Hz was applied to this segment, and the resulting filtered signal was stored in the data vector d_{sys}.

2. **Compute the signal envelope for each d_{sys}**: In order to extract the amplitude-based feature, the signal envelope for each d_{sys} was computed by first calculating the absolute value of the Hilbert transform [17] of d_{sys}, and then applying a fourth-order Butterworth low-pass filter with a cutoff frequency of 51 Hz to it. The resulting signal envelope faithfully recreated the original signal shape of d_{sys}.

3. **Estimate systolic noise floor for each d_{sys}**: The 10th percentile value of the above signal envelope provided a good approximation of the noise level and was therefore used to estimate the noise floor for d_{sys}.

4. **Obtain vector of systolic amplitude estimates, A_{sys} and A_{norm}, for each subject**: To ensure S1 and S2 did not influence systolic amplitude computation, the first 25% and last 15% of the signal envelope obtained in Step 2 were removed. The 60th percentile value of the remaining signal envelope provided a good approximation of the systolic interval signal amplitude, A_{sys}, that was independent of any outlier excursions due to non-cardiac events. All A_{sys} values for a subject were then stored in the form of an A_{sys} vector. Each value in this A_{sys} vector was then divided by the mean noise floor estimate for that subject (the mean of all

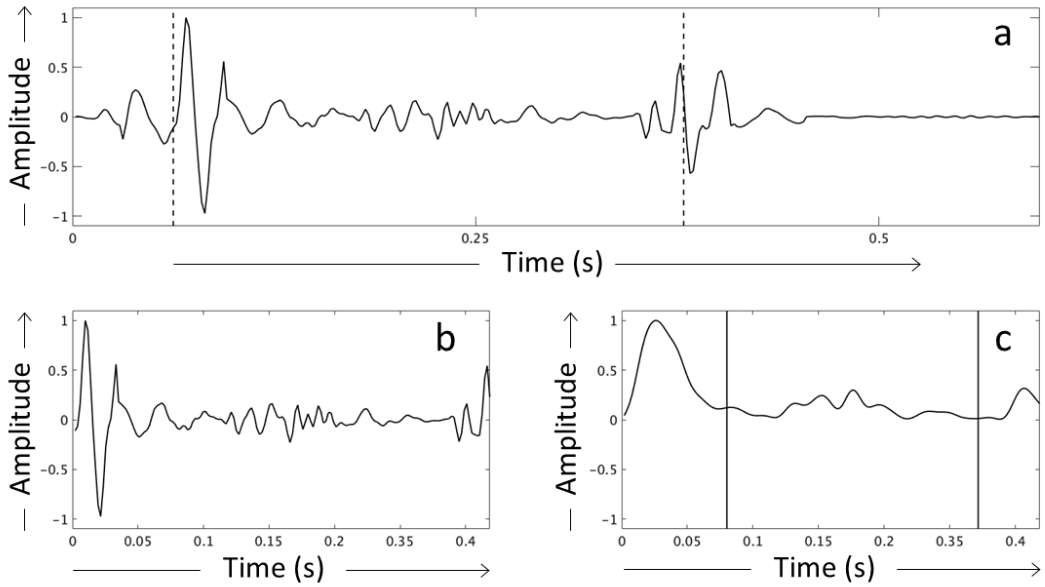

Figure 3-3 Example of amplitude-based-feature extraction. a) Normalized signal amplitude for the denoised phonocardiogram signal belonging to one heartbeat. The signal segment between the vertical dotted lines corresponding to the second half of S1, entire systolic interval, and the first half of S2 was extracted in the form of a d_{sys} vector. b) Normalized signal amplitude for extracted d_{sys} vector. c) Signal envelope for the signal in (b) calculated after applying a lowpass filter to the Hilbert transform of d_{sys}. The noise floor was estimated as the 10th percentile value of this signal envelope, and the systolic amplitude was estimated as the 60th percentile value of the signal envelope between the two vertical lines.

values for a subject obtained in Step 3) and then stored in the form of an A_{norm} vector. These vectors were used in Step 7 to compute the amplitude-based feature.

5. **Compute the frequency distribution for each d_{sys}**: The single-sided frequency distribution for each d_{sys} was required to compute the frequency-based feature. Since the systolic murmur for aortic stenosis was expected to be most prominent during mid-systole [1], a 64-point discrete Fourier transform was computed for the

middle 125 milliseconds (64 samples) of d_{sys} after application of a Hamming window to obtain this distribution (Figure 3-4).

6. **Obtain vector of high-frequency estimate, f_{com}, for each subject**: The high-frequency content in each frequency distribution was estimated by computing its frequency center of mass as:

$$f_{com} = \sum_{i=3}^{21}(x_i\, p_i) \Big/ \sum_{i=3}^{21}(p_i) \quad , \qquad (1)$$

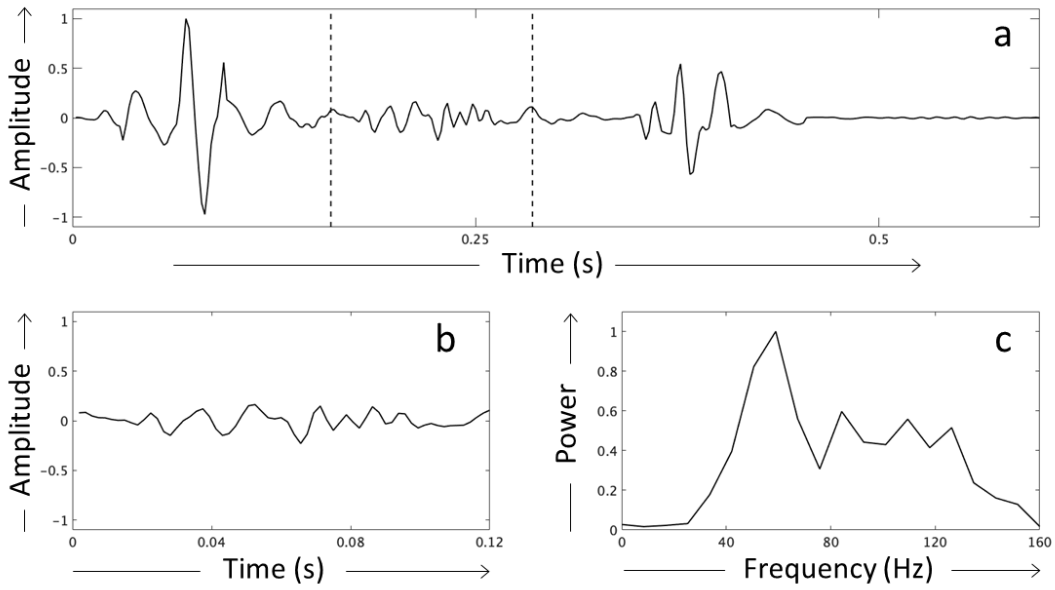

Figure 3-4 Example of frequency-based-feature extraction. a) Normalized signal amplitude for the denoised phonocardiogram signal belonging to one heartbeat. The signal segment between the vertical dotted lines corresponding to the middle 125 milliseconds of the dsys vector was used for extracting the frequency-based feature. b) Normalized signal amplitude for the extracted middle 125 milliseconds of the dsys vector. c) Frequency distribution for the signal in (b) calculated using a discrete Fourier transform after applying a Hamming window to it. The high-frequency content for the signal was estimated using the center of mass of the frequency distribution.

where p_i and x_i were the amplitude and frequency of the i^{th} bin in the discrete Fourier transform, and limits 3 and 21 corresponded to the frequencies 16 and 160 Hz, respectively. All frequency center of mass values for a subject were then stored in the form of an f_{com} vector. This vector was used in Step 7 to compute the frequency-based feature.

7. **Calculate the amplitude feature, A, and frequency feature, F_{com}, for each subject**: Not all heartbeats in a subject were expected to exhibit systolic murmurs due to variations in underlying physiology and sensor coupling. Therefore, the 85th percentile value of each of the A_{sys}, A_{norm}, and f_{com} vectors were chosen to represent individual A_{sys}, A_{norm}, f_{com} values for each subject. These individual A_{sys}, A_{norm}, and f_{com} values for all 96 subjects were then standardized by subtracting the mean and dividing by standard deviation. The resulting standardized A_{sys} and A_{norm} values were then summed to yield a single systolic amplitude feature, A. The resulting standardized f_{com} values were designated as the frequency feature, F_{com}. One A and F_{com} value each were available for each of the 96 subjects.

3.4 Diagnostic Results

Subjects with aortic stenosis were expected to show both high systolic signal amplitudes (measured by A) and elevated levels of systolic high-frequency content (measured by F_{com}) (Figure 3-5). This was visualized in a scatter plot of standardized

center-of-mass of systolic frequency distribution (F_{com}) vs. standardized systolic envelope amplitude (A) for all 96 subjects (Figure 3-6). Subjects with aortic stenosis visibly clustered in the top-right quadrant, whereas subjects with systolic murmurs due to other conditions exceeded the threshold on A but not on F_{com} and hence appeared in the bottom-right quadrant. For diagnostic purposes, a subject was classified as having aortic stenosis if their A and F_{com} values exceeded thresholds of 0.7 and –1.0, respectively. 11 of 12 aortic stenosis subjects and 80 of 84 non-aortic stenosis subjects had standardized

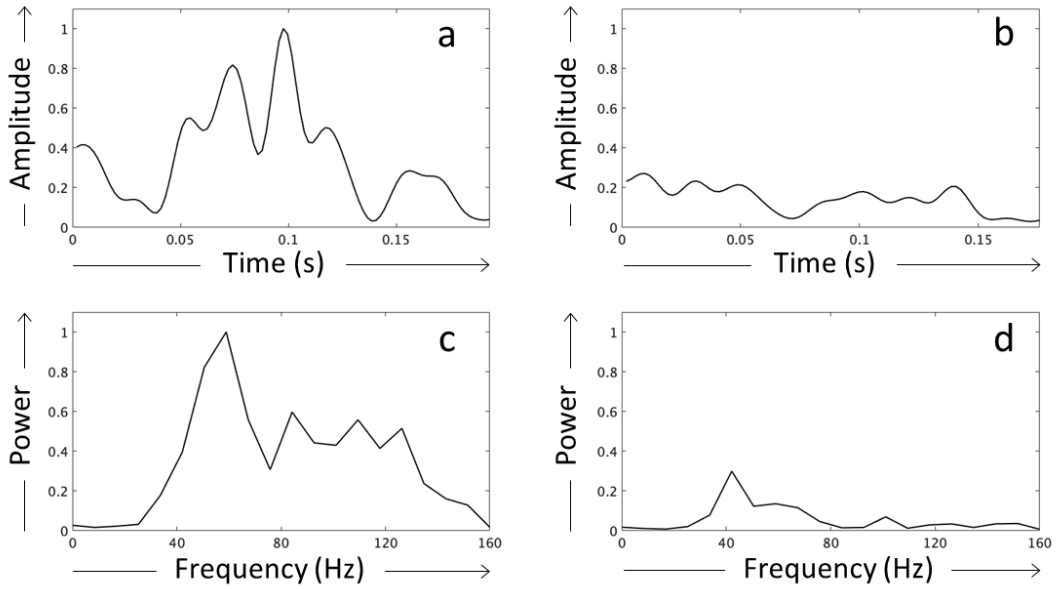

Figure 3-5 Comparison of feature extraction in aortic stenosis (a, c) and non-aortic-stenosis (b, d) subjects. a) Normalized systolic envelope amplitude for an aortic stenosis subject, showing a mid-systolic murmur and A = 3.4. b) Normalized systolic envelope amplitude for a non-aortic-stenosis subject showing A = 0.41. c) Normalized systolic frequency distribution for an aortic stenosis subject, showing elevated high-frequency content and F_{com} = 3.4. d) Normalized systolic frequency distribution for a non-aortic-stenosis subject showing F_{com} = —1.06.

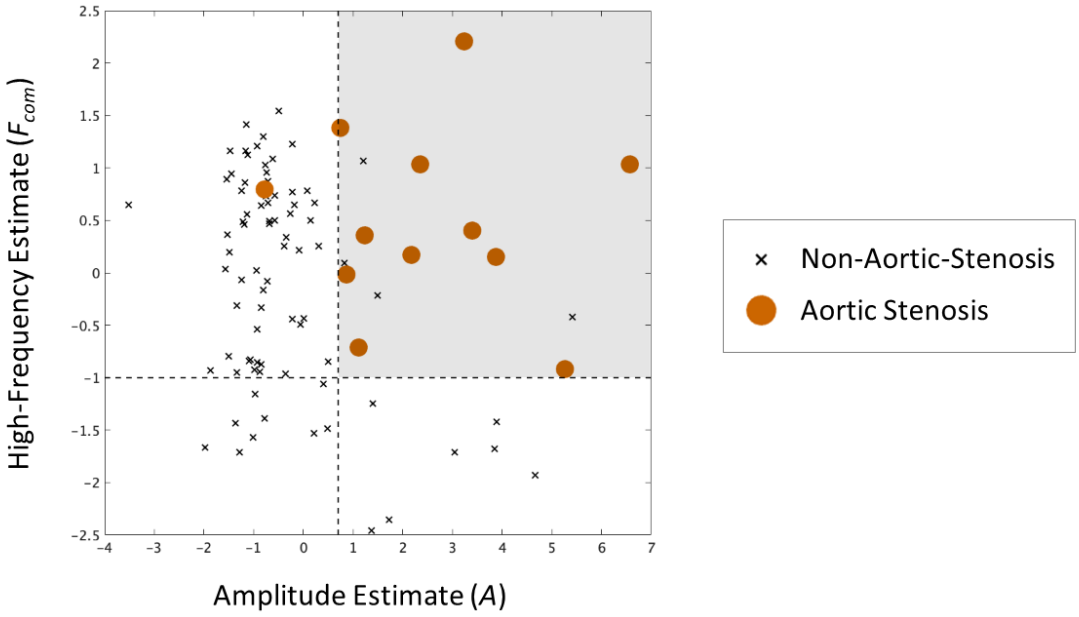

Figure 3-6 Standardized center-of-mass of systolic frequency distribution (F_{com}) vs. standardized systolic envelope amplitude (A) for n=96 subjects. Diagnostic criteria are shown as dashed lines. 11 of 12 aortic stenosis subjects and 4 of 84 non-aortic-stenosis subjects had $F_{com} > -1.0$ and $A > 0.7$. Aortic stenosis subjects visibly cluster in the top-right quadrant (shaded box), whereas non-aortic-stenosis subjects exhibiting other systolic-murmur inducing conditions exceeded threshold on A but not on F_{com}, and hence appeared in the bottom-right quadrant.

feature values above both diagnostic thresholds, corresponding to a sensitivity of 92% and specificity of 95%.

The complementary nature of the two features was observed by applying either threshold first and then performing a standard receiver operating characteristic (ROC) analysis of the other feature for the remaining set of subjects (Figure 3-7). For example, applying the $F_{com} > -1.0$ criteria removed 16 subjects, and ROC analysis of the amplitude-based feature for the remaining set of 80 subjects yielded an area under the curve (AUC) value of 0.94. Similarly, ROC analysis of the frequency-based feature for the set of 22

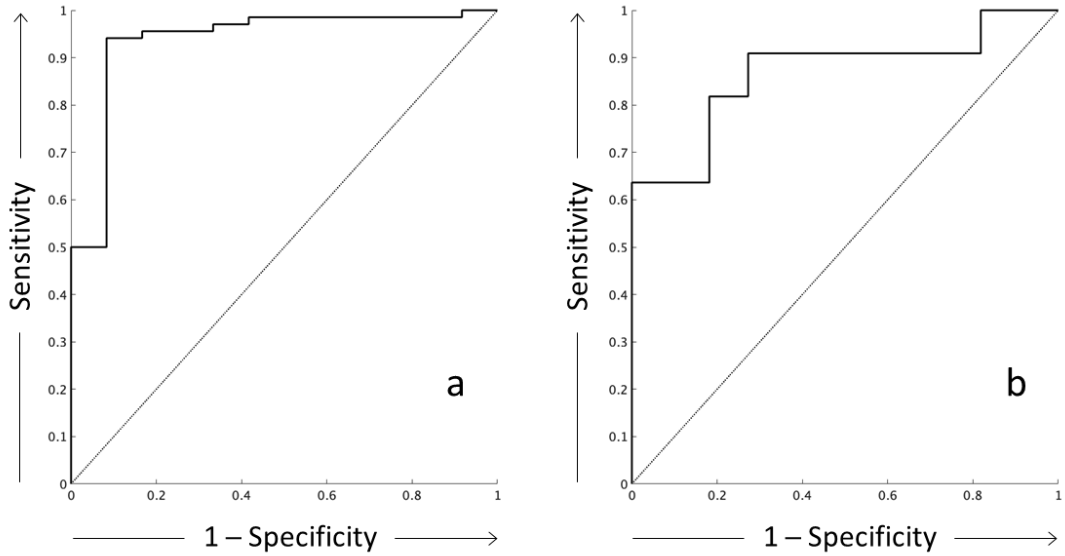

Figure 3-7 Receiver operating characteristic (ROC) curves on the amplitude (a) and frequency-based (b) features. a) ROC curve on the amplitude-based feature (A) for subjects with $F_{com} > -1.0$ yielded an area under the curve value of 0.94. b) ROC curve on the frequency-based feature (F_{com}) for subjects with A > 0.7 yielded an area under the curve value of 0.87.

subjects with $A > 0.7$ yielded an AUC value of 0.87. These high AUC values confirmed that the frequency-based feature provided significant complementary information to the amplitude-based feature, and that the two features were independently informative and specific to aortic stenosis.

The end-to-end phonocardiogram signal processing, feature extraction, and classification algorithms operated in a fully automated fashion with a per-subject computational runtime of 6 to 125 seconds on a 2.3 GHz Intel Core i7 processor (mean runtime of 52±22 seconds). This demonstrates the utility of the proposed phonocardiogram-based system in offering the healthcare provider a clinically relevant

heart disease diagnosis within minutes of acquiring signals in the real-world environment of a hospital, thereby allowing the diseased individual to embark on an accelerated path of care.

CHAPTER 4

EVALUATING HEART DISEASE

4.1 Goal: Evaluating Heart Failure

While diagnosing a heart disease involved establishing its presence or absence, evaluating a heart disease involved assessing its underlying etiology, severity, and effects [3]. Two criteria were set forward while searching for a disease to validate the evaluative capability of the proposed phonocardiogram-based system: first, this disease must be prevalent enough to benefit from evaluation at the point of primary care, and second, this disease must currently be evaluated using tools that might be unavailable in low-resource settings due to lack of training and experience for operating these.

Heart failure – characterized by structural or functional impairment of ventricular filling or ejection of blood [18] – is one such disease that satisfied both the above criteria.

20% to 45% of the American population above 45 years of age is at risk of developing heart failure during their lifetime, and around 4 of 10 heart failure patients are at a risk of mortality within the first 5 years of diagnosis [4]. Heart failure may be a result of a spectrum of disorders, the most common being left ventricular diastolic dysfunction present in around half the cases [18]. In these individuals, the left ventricle shows increased chamber stiffness and impaired relaxation which renders it unable to accept blood during diastole [18] [19].

Evidence of left ventricular diastolic dysfunction is obtained through 2-dimensional and Doppler echocardiography and involves the calculation of several parameters to assess left ventricular dimensions, wall motion, ejection fraction, and valvular blood-flow patterns [19]. Cutoff values for these parameters are then analyzed to determine the degree of diastolic dysfunction and to estimate left ventricular filling pressures [19]. While a physician can independently analyze these echocardiographic parameters, the calculation of these indices requires interpretation of echocardiographic images by a credentialed sonographer [20]. These sonographers undergo regular training and education to ensure quality and consistency in image interpretation [20]. Echocardiography is therefore a resource-intense tool that might be unavailable in low resource primary care settings. In these settings, a tool that can aid the physician in evaluating left ventricular diastolic function without requirements of training and experience in operating it therefore carries great potential in accelerating the path of care

in individuals with heart failure. This was the evaluative goal for the proposed phonocardiogram-based system.

4.2 Subject Population

The phonocardiogram and electrocardiogram signals used to validate analytical methods for this purpose were collected after obtaining informed consent from 34 adult inpatients scheduled for right heart catheterization at the Oregon Health & Science University Hospital (Portland, OR) between 2018 and 2019 (Institutional Review Board Number: 19067). The subjects included 13 females and 21 males between 24 and 84 years of age (mean age of 62±17 years, age data available for n=23 subjects) with left ventricular ejection fraction values between 5% and 78% (mean ejection fraction value of 49±17%, data available for n=30 subjects). Signal acquisition lasted between 4 and 80 minutes per subject depending on the catheterization laboratory schedule. Echocardiographic reports from transthoracic examinations performed in close proximity to the right heart catheterization were obtained for each subject, and each report contained one or more of five parameters based on the quality of the study (Table 4-1). The availability of this real-world data and echocardiographic parameters further established the validity of this evaluative goal for demonstrating the potential of the proposed phonocardiogram-based system.

Parameter	Description	Observed Range	Number of Subjects
Peak E velocity	The peak early diastolic flow velocity measured at the mitral valve leaflet tips	0.42 – 1.55 m/s	26
E/A ratio	The ratio of early-to-late peak diastolic flow velocities measured at the mitral valve leaflet tips	0.66 – 3.66	18
e' velocity*	The average early diastolic flow velocity measured at the mitral valve annulus	0.03 – 0.17 m/s	23
Peak TR velocity	The peak regurgitant systolic jet velocity measured at the tricuspid valve	2.07 – 3.71 m/s	22
LAVi	The maximum left atrial volume indexed to body surface area	14.2 – 85.8 ml/m^2	25

*Table 4-1 Summary of parameters available in echocardiographic reports. *Derived indirectly by dividing each peak E velocity parameter value by the available tissue Doppler imaging E/e' ratio parameter value.*

4.3 Feature Extraction

Left ventricular diastolic function evaluation was carried out by computing phonocardiogram-based proxies for the five echocardiographic parameters. Proxy metric

computation involved extraction of features that characterized physiological phenomena such as cardiac pressure gradients, muscle motion, and blood flow that were otherwise measured by the echocardiographic parameters [19]. The clinical value of these proxy metrics was determined using an algorithm described in the joint recommendations of the American Society of Echocardiography (ASE) and the European Association of Cardiovascular Imaging (EACVI) in 2016 [19] (Figure 4-1). The first part of this algorithm used peak E velocity, e' velocity, peak TR velocity, and LAVi parameters to identify left ventricular diastolic dysfunction in subjects with normal left ventricular ejection fraction values. The second part of this algorithm used the above four parameters along with the E/A ratio parameter to estimate left atrial pressure (as an indirect measurement of left ventricular filling pressure) in subjects with reduced ejection fraction values or in those with normal left ventricular ejection fraction values in the presence of underlying myocardial disease. Ground truth diastolic dysfunction and left atrial pressure evaluations were obtained for each subject using their echocardiographic parameters irrespective of their ejection fraction value. For each of these evaluations, subjects were assigned to be either "afflicted" (presence of diastolic dysfunction, or presence of elevated left atrial pressure), "normal", or "indeterminate", with the "indeterminate" evaluation reserved for subjects with discordant echocardiographic parameters or those that required evaluation beyond the scope of the algorithm [19] [21]. For subjects with "afflicted" or "normal" ground truths, the corresponding phonocardiogram-based evaluations were obtained using the computed proxy metrics. The accuracies of proxy metric-based diastolic

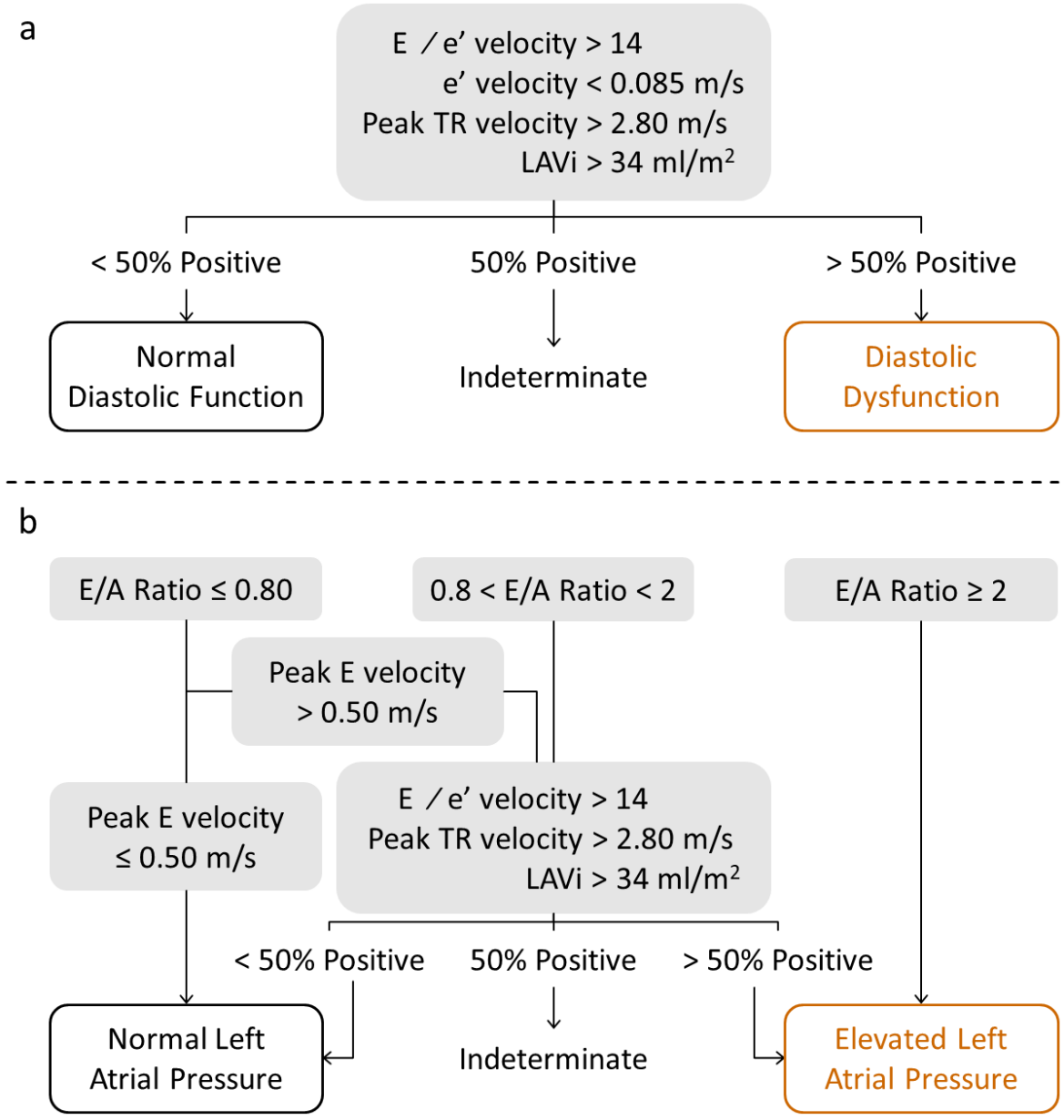

Figure 4-1 The algorithm described in the joint recommendations of the American Society of Echocardiography and the European Association of Cardiovascular Imaging in 2016 for left ventricular diastolic function (a) and mean left atrial pressure (b) evaluation. The cutoff value for "average" e' velocity was chosen as the mean of those for "lateral" and "septal" e' velocities.

function and left atrial pressure evaluations were then determined by calculating their

sensitivity and specificity against echocardiographic parameter-based ground truths.

For this purpose, the filtering, noise subtraction, heartbeat segmentation, and heartbeat quality assurance algorithms described in Chapter 2 were applied to phonocardiogram signals acquired from the n=34 subject set. Signals recorded at the aortic, pulmonic, and mitral auscultation points were chosen for this analysis depending on the proxy metric being computed. Feature extraction for proxy metric computation utilized either raw or denoised phonocardiogram signals belonging to either all or exclusively high-quality heartbeats depending on the underlying physiology being characterized (Table 4-2). Three types of features were extracted from the systolic or diastolic signal interval of each heartbeat: an amplitude-based feature, a frequency-based feature, and a spectral entropy-based feature. For calculating the amplitude-based feature, a Hilbert transform [17] was applied to the selected phonocardiogram signal segment followed by the application of a fourth-order Butterworth low-pass filter with a cutoff frequency of 51 Hz. The amplitude-based feature was then calculated as the 60^{th} percentile value of this signal envelope (like A_{sys} calculation in Chapter 3) and was used to compute the proxy metric for the peak E velocity parameter. For calculating the frequency-based feature, a 64-point discrete Fourier transform was calculated from the selected phonocardiogram signal segment after application of a Hamming window. The frequency-based feature was then calculated as the center-of-mass for the frequency distribution between 16 and 160 Hz (like f_{com} calculation in Chapter 3) and was used to compute the proxy metrics for e' velocity and LAVi parameters. The spectral entropy

Parameter	Type of Phono-cardiogram Signal used	Type of Heartbeats used	Segment of Phono-cardiogram Signal used for Feature Extraction	Feature used to Compute Proxy Metric
Peak E velocity	Denoised	High-quality	Diastolic interval	Ratio of pulmonic-to-aortic signal amplitude
E/A ratio	Raw	High-quality	Diastolic interval (early = first half, late = second half)	Ratio of early-to-late pulmonic spectral entropy
e' velocity	Denoised	All	Second half of systolic interval	Aortic frequency center of mass
Peak TR velocity	Denoised	High-quality	Diastolic interval	Ratio of pulmonic-to-aortic spectral entropy
LAVi	Raw	All	First half of diastolic interval	Mitral frequency center of mass

Table 4-2 Summary of features extracted to compute proxies for each echocardiographic parameter.

feature was calculated as the negative product of the signal probability distribution for the selected phonocardiogram signal segment with its logarithm [22] and was used to compute the proxy metrics for E/A ratio and peak TR velocity parameters.

Peak E velocity: This parameter was a measure of peak early diastolic flow velocity at the mitral valve leaflet tips during passive emptying of the left atrium into the left ventricle [19]. The value of this parameter reflected the pressure gradient between the left atrium and left ventricle and was affected by any alterations in the rate of left ventricular relaxation or left atrial pressure [19]. As seen in Chapter 3, subjects with high flow velocities showed corresponding high signal amplitudes. The ratio of pulmonic-to-aortic amplitude-based features calculated for the diastolic denoised phonocardiogram signals in high-quality beats was therefore chosen to characterize this trend. Since the direction of diastolic blood flow was away from the location of aortic and pulmonic auscultation points, lower amplitude-based feature values were seen for high peak E velocity values. The ratio of pulmonic-to-aortic feature values here allowed for the comparison of this trend on the left and right sides of the heart. As a result, greater diastolic amplitude ratios were seen for subjects with larger peak E velocity values, and this ratio was therefore chosen to compute the proxy metric for the peak E velocity parameter.

E/A ratio: This parameter was a measure of the ratio of early-to-late peak diastolic flow velocities at the mitral valve leaflet tips during the passive and subsequent active emptying of the left atrium into the left ventricle [19]. The value of this parameter was used to identify the state of left ventricular function: normal, impaired relaxation, moderate diastolic dysfunction (pseudoformal filling), or restrictive left ventricular filling (impaired left ventricular compliance) [19]. Diastolic phonocardiogram signal segments

associated with left ventricular filling-related muscular contractions were identified using the spectral-entropy based feature. Lower spectral entropy values were seen in late-diastolic signal segments corresponding to active left atrial contractions when compared to early-diastolic signal segments corresponding to passive left atrial emptying. This trend was strongest for raw phonocardiogram signals in high-quality heartbeats acquired at the pulmonic auscultation point. A ratio of early-to-late pulmonic diastolic signal spectral entropy-based features was therefore chosen to compute the proxy metric for the E/A ratio parameter.

e' velocity: This parameter was a measure of the average early diastolic flow velocity at the mitral valve annulus during passive emptying of the left atrium into the left ventricle [19]. The value of this parameter was seen to be associated with the time constant of left ventricular relaxation [19]. The left ventricular hemodynamic forces responsible for these early-diastolic mitral annulus deflections were indirectly estimated during systole. While high-frequency vibrations associated with high-velocity blood flow showed corresponding elevated levels of high-frequency signal content (as seen in Chapter 3), low-frequency vibrations associated with cardiac muscle motion showed corresponding elevated levels of low-frequency signal content [23]. Subjects with high e' velocity values due to larger mitral annulus deflections also showed greater muscle motion-related low frequency content during systole. This phenomenon was characterized by calculating the frequency-based feature for the denoised end-systolic

phonocardiogram signals in all heartbeats acquired at the aortic auscultation point. This feature was therefore chosen to compute the proxy metric for the e' velocity parameter.

Peak TR velocity: This parameter was a measure of the peak regurgitant systolic jet velocity at the tricuspid valve during right ventricular contraction [19]. The value of this parameter provided an indirect measure of the pulmonary artery systolic pressure which was seen to be directly correlated to left atrial pressure [19]. Subjects with greater peak TR velocity values and therefore higher pulmonary artery pressures have been observed to show organized heart sound patterns in phonocardiogram signals collected at the pulmonic auscultation point [11]. These patterns were characterized by calculating the ratio of the spectral entropy-based feature for the diastolic interval phonocardiogram signal acquired at the pulmonic and aortic auscultation points. Lower spectral entropy values were seen at the pulmonic auscultation point for subjects with greater peak TR velocity values. This trend was strongest for denoised phonocardiogram signals in high-quality heartbeats, and this ratio was therefore chosen to compute the proxy metric for the peak TR velocity parameter.

LAVi: This parameter was a measure of the maximum left atrial volume indexed to body surface area [19]. The value of this parameter reflected the cumulative effects of increased left atrial pressures over time [19]. Subjects with greater LAVi values and therefore larger left atria showed greater muscle-motion related low-frequency signal content during left ventricular filling in early diastole. This trend was characterized by calculating the frequency-based feature for the early diastolic interval phonocardiogram

Proxy Metric	Number of Subjects	R^2-value	*p*-value	Bland-Altman Bias and Limits of Agreement
Peak E velocity	20	0.47	0.0009	0.00 ± 0.64 m/s
E/A ratio	18	0.58	0.0003	-0.03 ± 1.24
e' velocity	20	0.49	0.0006	0.01 ± 0.06 m/s
Peak TR velocity	16	0.51	0.0018	-0.05 ± 0.89 m/s
LAVi	24	0.44	0.0004	-1.0 ± 31.5 ml/m^2

Table 4-3 Statistical measures for phonocardiogram-based proxy metrics.

signal acquired at the mitral auscultation point and was strongest for raw phonocardiogram signals in all heartbeats. This feature was therefore chosen to compute the proxy metric for the LAVi parameter.

Individual per-heartbeat feature values were averaged to obtain one mean feature value per-parameter per-subject. These per-subject feature values were then plotted against their corresponding echocardiographic parameter values, and the proxy metric was calculated using a linear fit (Table 4-3 and Figure 4-2). Each proxy metric was adjusted by subtracting the linear model's intercept and dividing by its slope, and those proxy values that were outside physiologically feasible ranges were truncated accordingly. Proxy metrics could not be computed for all subjects either due to absence of

corresponding parameters in their echocardiographic reports or due to occasional signal quality deficiencies during measurement in the noisy catheterization laboratory environment. These metrics were therefore unavailable for peak E velocity and peak TR velocity parameters in 6 subjects each, for the e' velocity parameter in 3 subjects, and for the LAVi parameter in 1 subject.

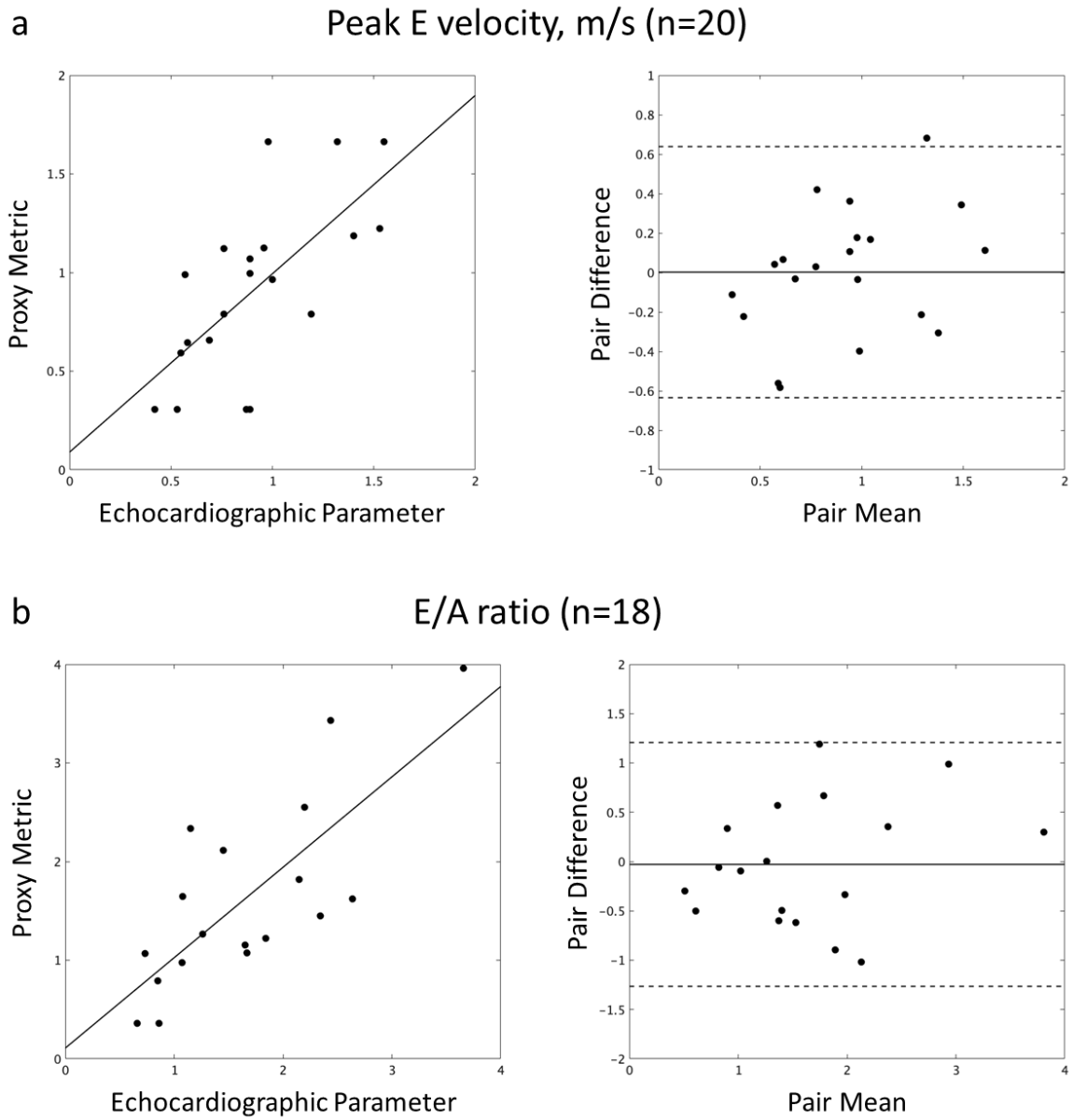

(Figure 4-2 continued from previous page)

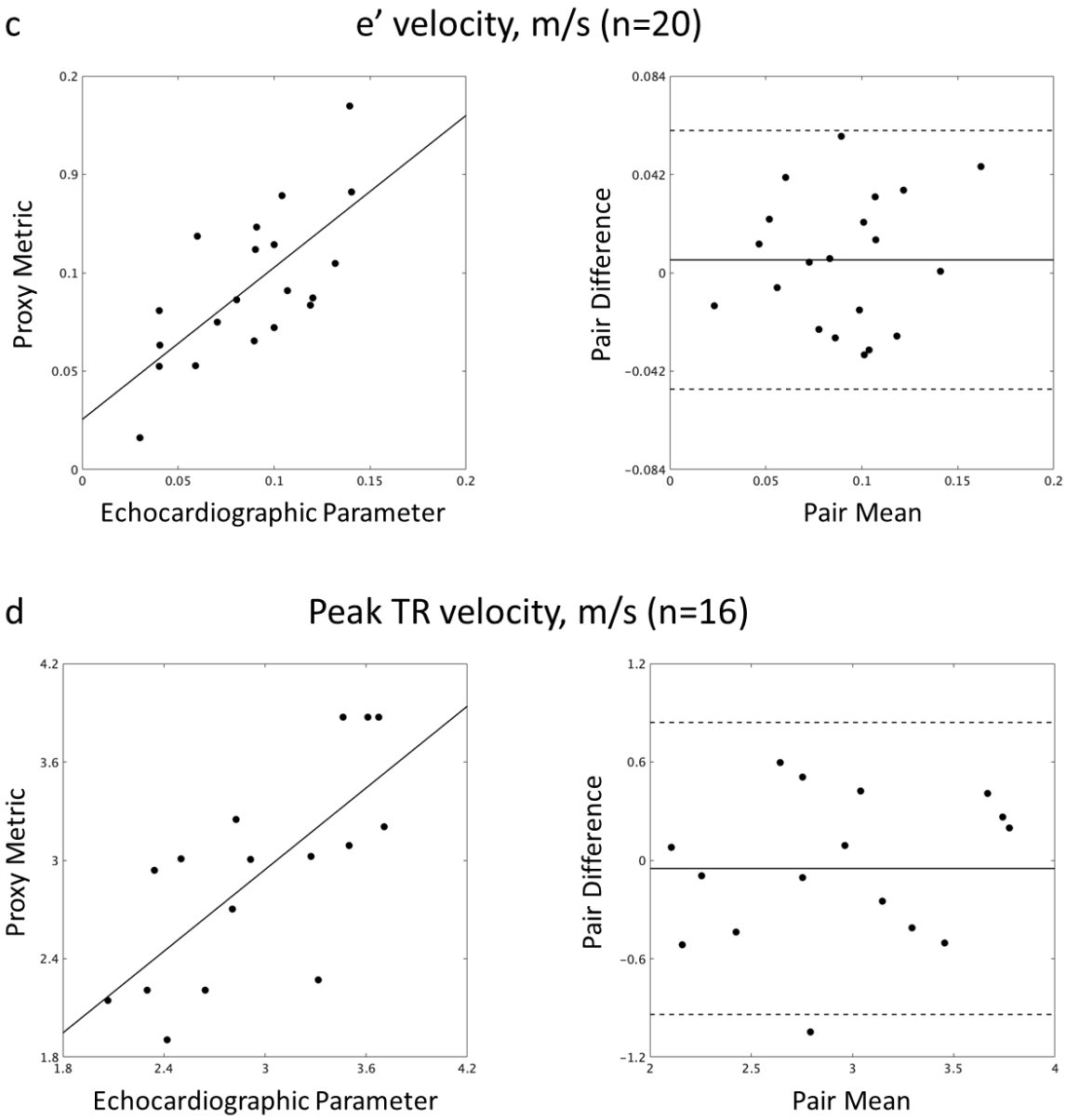

(Figure 4-2 continued next page)

(Figure 4-2 continued from previous page)

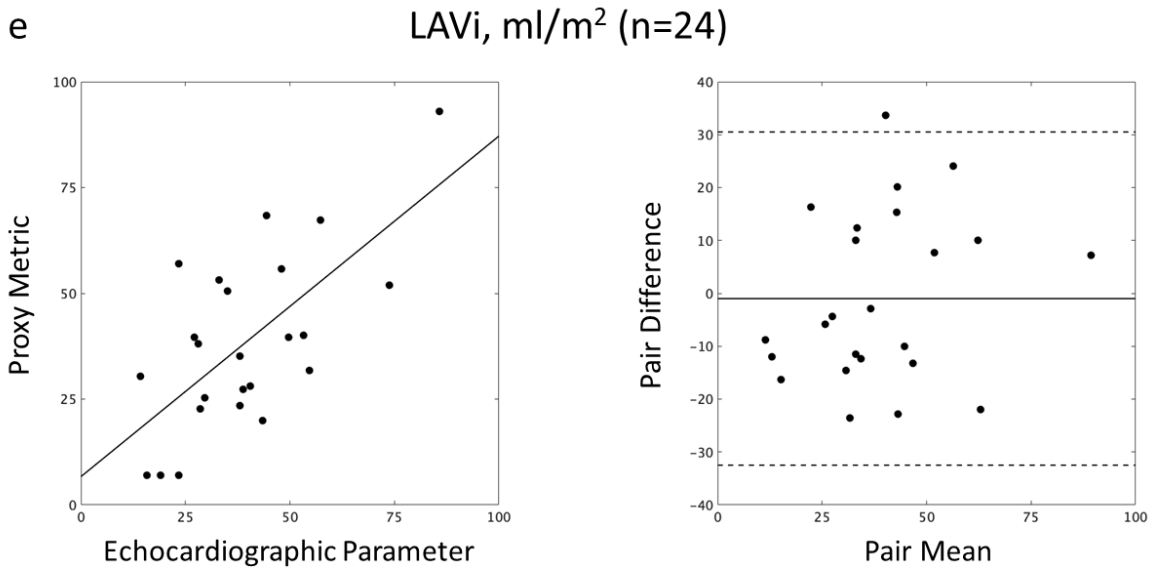

Figure 4-2 Proxy metric vs. echocardiographic parameter scatter plots (left column) and Bland-Altman plots (right column) for peak E velocity (a), E/A ratio (b), e' velocity (c), peak TR velocity (d), and LAVi (e). Markers represent subjects. Scatter plots show solid linear regression lines and Bland-Altman plots show bias (horizontal solid line) and 95% limits of agreement (horizontal dotted lines), also summarized in Table 4-3.

4.4 Evaluative Results

Echocardiographic parameter-based ground truth evaluations for left ventricular diastolic function obtained by applying the 2016 ASE/EACVI algorithm were available for 29 of 34 subjects, with 12 subjects showing diastolic dysfunction and 17 subjects showing normal diastolic function. Proxy-metric based evaluations were "indeterminate" for 5 of these 29 subjects. For the remaining 24 subjects, the sensitivity and specificity for proxy

metric-based left ventricular diastolic function evaluation were 70% and 100% (Figure 4-3). Similarly, echocardiographic parameter-based ground truth evaluations for left atrial pressure were available for 17 of 34 subjects, with 11 subjects showing elevated left atrial pressures and 6 subjects showing normal left atrial pressures. Proxy-metric based evaluations were "indeterminate" for 5 of these 17 subjects. For the remaining 12 subjects, the sensitivity and specificity for proxy metric-based left atrial pressure evaluation were 75% and 75%. The overall evaluative accuracy for this phonocardiogram-based system was 87.5% for evaluating left ventricular diastolic function and 75% for evaluating left atrial pressures. These results were closely in line with those reported in studies comparing evaluative accuracy of echocardiographic parameters with gold-standard catheter-based pressure measurements [24].

The end-to-end phonocardiogram signal processing, feature extraction, and proxy metric computation algorithms for left ventricular diastolic function evaluation operated in a fully automated manner without expert supervision. While the clinical value of the proxy metrics was determined using the 2016 ASE/EACVI algorithm, the proxy metric computation itself was independent of this algorithm and therefore immune to any guideline modifications that might be introduced in the future. This demonstrates the utility and potential of the proposed phonocardiogram-based system in providing echocardiography-like parameters to the interpreting physician within minutes of signal acquisition in the real-world environment of a hospital, thereby allowing individuals with heart failure to embark on an accelerated path of care.

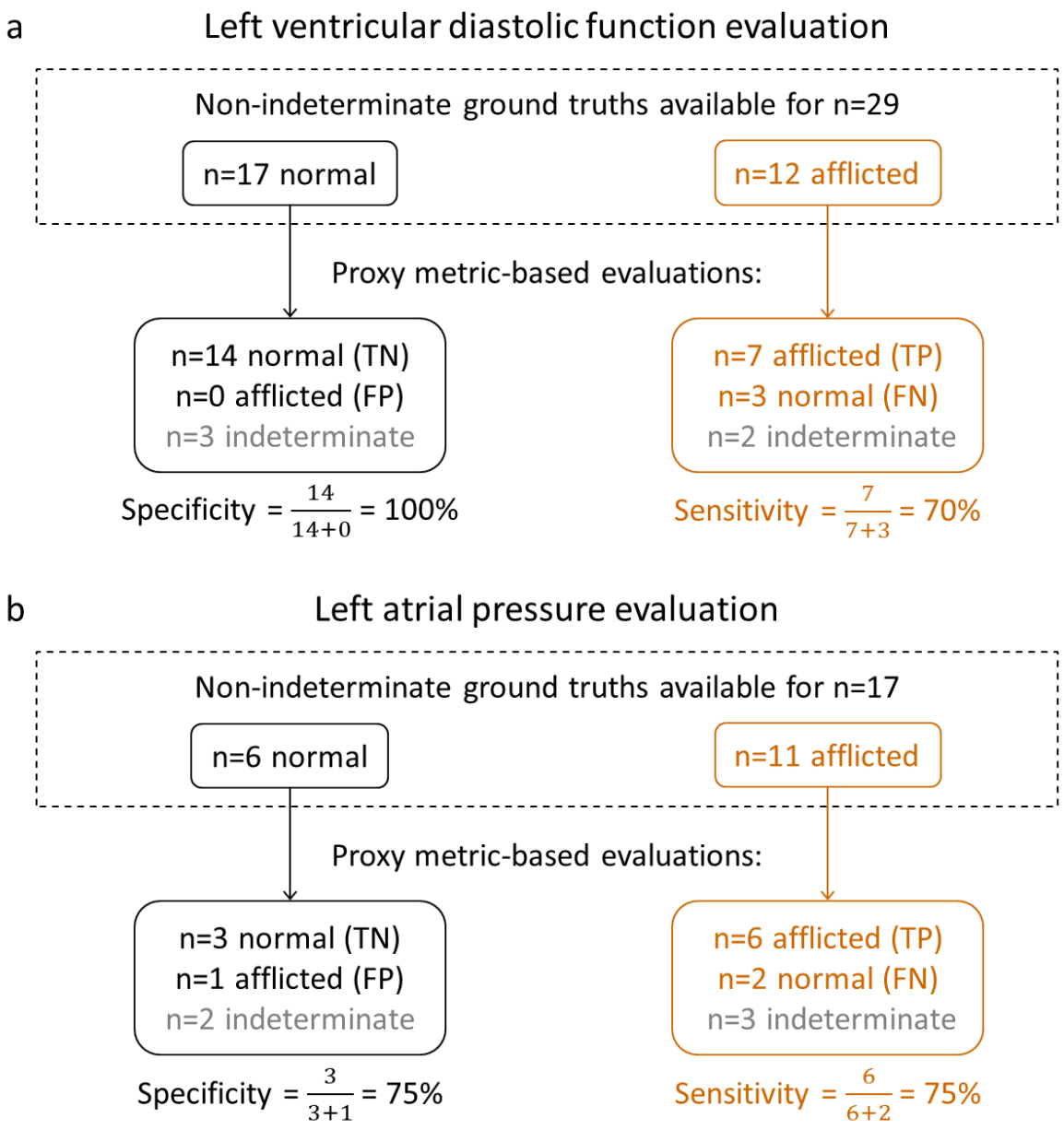

Figure 4-3 Summary of left ventricular diastolic dysfunction (a) and left atrial pressure (b) evaluations for 34 subjects. a) Echocardiographic parameter-based ground truth left ventricular diastolic function evaluations were available for 29 subjects. The overall evaluative accuracy of proxy metrics was 87.5%. b) Echocardiographic parameter-based ground truth left atrial pressure evaluations were available for 17 subjects. The overall evaluative accuracy of proxy metrics was 75%. (TN=True negatives, FP=False positives, TP=True positives, FN=False negatives).

CHAPTER 5

CONCLUSION

5.1 Impact of the Presented System

Every 10 years since the late 1990's, the American Heart Association has updated its mission statement to set forward new research, advocacy, and public health goals for the upcoming decade [5]. Over the past 20 years, these guidelines have focused on decreasing risk factors for heart disease such as obesity, diabetes, and hypertension as well as promoting healthy behaviors such as regular physical activity, maintaining a healthy weight, and smoking cessation [5]. The 2020-30 guidelines expand on this mission and call for an equitable increase in healthy life expectancy through the prevention of premature death due to heart disease [5]. Achieving this goal requires the use of evidence-based preventive tools capable of early identification and effective management of heart disease [7]. While existing diagnostic and evaluative tools come close to filling this need, these are either limited in their capability, require extensive training and experience for their use, or are unavailable in low-resource settings. This

poses a challenge in the successful realization of the 2030 American Heart Association goals, especially in the early diagnosis of individuals who may otherwise experience sudden death or in the timely evaluation of individuals who may otherwise continue to live with disease-related disabilities. The phonocardiogram-based system presented here was shown to overcome these challenges to provide clinically relevant heart disease diagnosis and evaluation at the point of primary care. This system analyzed phonocardiogram signals acquired noninvasively and operated in a fully automated end-to-end manner without any expert supervision. Its operation was based on fundamental principles of physiology and its potential was demonstrated through the diagnosis of aortic stenosis in 96 subjects and the evaluation of left ventricular diastolic function in 34 subjects. Diagnostic and evaluative results from the use of this system were produced within minutes of signal acquisition without requirements for any follow-up visits and were comparable to those from existing risk assessment tools and advanced imaging modalities. This system offers great value as part of the primary care provider's toolkit and carries great potential in improving a patient's care outcomes.

5.2 Recommendations for Future Development

The filtering, noise subtraction, heartbeat segmentation, heartbeat quality assurance, and feature extraction algorithms presented here can be leveraged to diagnose and evaluate other heart disease conditions. For example, the systolic murmur identification technique created for aortic stenosis can be extended to other valvular and

congenital heart disease. Proxy metric computation techniques developed for left ventricular diastolic function evaluation can be used for evaluating pulmonary hypertension and left ventricular size, or for calculating left ventricular stroke volume or cardiac output. These techniques can also be used to evaluate the health of coronary arteries or to ensure proper functions of prosthetic valves and grafts. This system can also be used to establish the presence of any comorbidities in a pre-diagnosed disease or as part of the pre- or post-operative evaluation of inpatients. Future validation goals could expand on existing subject counts and adapt this system into a portable form factor for evaluating the heart's exercise-response or for use in telemedicine visits for vulnerable patients.

REFERENCES

[1] J. E. Hall, Guyton and Hall Textbook of Medical Physiology, Elsevier, 2015.

[2] D. K. Arnett et al., "2019 ACC/AHA Guideline on the Primary Prevention of Cardiovascular Disease: A Report of the American College of Cardiology/American Heart Association Task Force on Clinical Practice Guidelines," *Circulation,* vol. 140, no. 11, pp. e596-e646, 2019.

[3] A. H. Goroll and A. G. Mulley, Primary Care Medicine: Office Evaluation and Management of the Adult Patient, Wolters Kluwer Health, 2014.

[4] S. S. Virani et al., "Heart Disease and Stroke Statistics—2020 Update: A Report From the American Heart Association," *Circulation,* vol. 141, no. 9, pp. e139-e596, 2020.

[5] S. Y. Angell et al., "The American Heart Association 2030 Impact Goal: A Presidential Advisory From the American Heart Association," *Circulation,* vol. 141, no. 9, pp. e120-e138, 2020.

[6] M. McClellan, N. Brown, R. M. Califf, and J. J. Warner, "Call to Action: Urgent Challenges in Cardiovascular Disease: A Presidential Advisory From the American Heart Association," *Circulation,* vol. 139, no. 9, pp. e44-e54, 2019.

[7] J. J. Warner et al, "Advancing Healthcare Reform: The American Heart Association's 2020 Statement of Principles for Adequate, Accessible, and Affordable Health Care: A Presidential Advisory From the American Heart Association," *Circulation,* vol. 141, no. 10, pp. e601-e614, 2020.

[8] B. E. White et al., "Abstract 13831: Handheld Wireless Digital Phonocardiography for Machine Learning-Based Detection of Mitral Regurgitation," *Circulation,* vol. 140, no. Suppl_1, p. A13831, 2019.

[9] L.S. Lai, A. N. Redington, A. J. Reinisch, M. J. Unterberger, and A. J. Schriefl, "Computerized Automatic Diagnosis of Innocent and Pathologic Murmurs in Pediatrics: A Pilot Study," *Congenital Heart Disease,* vol. 11, no. 5, pp. 386-395, 2016.

[10] H.-M. Tsao et al., "Early Detection of Electromechanical Dysfunction in Patients with Idiopathic Premature Ventricular Contractions," *Pacing and Clinical Electrophysiology,* vol. 42, no. 6, pp. 637-645, 2019.

[11] M. Elgendi et al., "The Voice of the Heart: Vowel-Like Sound in Pulmonary Artery Hypertension," *Diseases,* vol. 6, no. 2, p. 26, 2018.

[12] U.S. Food & Drug Administration, 2018. [Online]. Available: https://www.accessdata.fda.gov/cdrh_docs/pdf17/K173156.pdf.

[13] N. Upadhyay, and A. Karmakar, "Speech Enhancement using Spectral Subtraction-type Algorithms: A Comparison and Simulation Study," *Procedia Computer Science,* vol. 54, pp. 574-584, 2015.

[14] Y.-C. Yeh, and W.-J. Wang, "QRS complexes detection for ECG signal: The Difference Operation Method," *Computer Methods and Programs in Biomedicine,* vol. 91, no. 3, pp. 245-254, 2008.

[15] P. Genereux et al., "Natural History, Diagnostic Approaches, and Therapeutic Strategies for Patients With Asymptomatic Severe Aortic Stenosis," *Journal of the American College of Cardiology,* vol. 67, no. 19, pp. 2263-2288, 2016.

[16] D.-H. Kang et al., "Early Surgery or Conservative Care for Asymptomatic," *The New England Journal of Medicine,* vol. 382, no. 2, pp. 111-119, 2020.

[17] M. Feldman, "Hilbert Transform in Vibration Analysis," *Mechanical Systems and Signal Processing,* vol. 25, no. 3, pp. 735-802, 2011.

[18] C. W. Yancy et al., "2013 ACCF/AHA Guideline for the Management of Heart Failure," *Circulation,* vol. 128, no. 16, p. e240–e327, 2013.

[19] S. F. Nagueh et al., "Recommendations for the Evaluation of Left Ventricular Diastolic Function by Echocardiography: An Update from the American Society of Echocardiography and the European Association of Cardiovascular Imaging," *Journal of the American Society of Echocardiography,* vol. 29, no. 4, pp. 277-314, 2016.

[20] M. H. Picard et al., "American Society of Echocardiography Recommendations for Quality Echocardiography Laboratory Operations," *Journal of the American Society of Echocardiography,* vol. 24, no. 1, pp. 1-10, 2011.

[21] J. G. Almeida et al., "Impact of the 2016 ASE/EACVI Recommendations on the Prevalence of Diastolic Dysfunction in the General Population," *European Heart Journal - Cardiovascular Imaging,* vol. 19, no. 4, pp. 380-386, 2018.

[22] Y. N. Pan, J. Chen, and X. L. Li, "Spectral Entropy: A Complementary Index for Rolling Element Bearing Performance Degradation Assessment," *Proceedings of the Institution of Mechanical Engineers, Part C: Journal of Mechanical Engineering Science,* vol. 223, no. 5, pp. 1223-1231, 2009.

[23] A. N. Pelech, "The Physiology of Cardiac Auscultation," *Pediatric Clinics of North America,* vol. 51, no. 6, pp. 1515-1535, 2004.

[24] B. Balaney et al., "Invasive Validation of the Echocardiographic Assessment of Left Ventricular Filling Pressures Using the 2016 Diastolic Guidelines: Head-to-Head Comparison with the 2009 Guidelines," *Journal of the American Society of Echocardiography,* vol. 31, no. 1, pp. 79-88, 2018.